RESEARCH REPORT

EJN European Journal of Neuroscience | FENS | WILEY

Inhibitory inputs to an inhibitory interneuron: Spontaneous postsynaptic currents and GABA$_A$ receptors of A17 amacrine cells in the rat retina

Pablo Beltrán-Matas [ID] | Áurea Castilho [ID] | Barbora Tencer [ID] | Margaret L. Veruki [ID] | Espen Hartveit [ID]

Department of Biomedicine, University of Bergen, Bergen, Norway

Correspondence
Margaret L. Veruki and Espen Hartveit, Department of Biomedicine, University of Bergen, Jonas Lies vei 91, N-5009 Bergen, Norway.
Email: margaret.veruki@uib.no and espen.hartveit@uib.no

Abstract

Amacrine cells constitute a large and heterogeneous group of inhibitory interneurons in the retina. The A17 amacrine plays an important role for visual signalling in the rod pathway microcircuit of the mammalian retina. It receives excitatory input from rod bipolar cells and provides feedback inhibition to the same cells. However, from ultrastructural investigations, there is evidence for input to A17s from other types of amacrine cells, presumably inhibitory, but there is a lack of information about the identity and functional properties of the synaptic receptors and how inhibition contributes to the integrative properties of A17s. Here, we studied the biophysical and pharmacological properties of GABAergic spontaneous inhibitory postsynaptic currents (spIPSCs) and GABA$_A$ receptors of A17 amacrines using whole-cell and outside-out patch recordings from rat retinal slices. The spIPSCs displayed fast onsets (10%–90% rise time ~740 μs) and double-exponential decays (τ_{fast} ~4.5 ms [43% of amplitude]; τ_{slow} ~22 ms). Ultra-fast application of brief pulses of GABA (3 mM) to patches evoked responses with deactivation kinetics best fitted by a triple-exponential function (τ_1 ~5.3 ms [55% of amplitude]; τ_2 ~48 ms [32% of amplitude]; τ_3 ~187 ms). Non-stationary noise analysis of spIPSCs and patch responses yielded single-channel conductances of ~21 and ~25 pS, respectively. Pharmacological analysis suggested that the spIPSCs are mediated by receptors with an α1βγ2 subunit composition and the somatic receptors have an α2βγ2 and/or α3βγ2 composition. These results demonstrate the presence

---

Abbreviations: AMPA, α-amino-3-hydroxy-5-methyl-4-isoxazolepropionic acid; CNQX, 6-cyano-7-nitroquinoxaline-2,3-dione; CPP, (RS)-3-(2-carboxypiperazin-4-yl)-propyl-1-phosphonic acid; E_{Cl}, chloride equilibrium potential; GABA, γ-aminobutyric acid; INL, inner nuclear layer; IR-DIC, infrared differential interference contrast; ONL, outer nuclear layer; OPL, outer plexiform layer; R_N, input resistance; R_s, series resistance; spEPSC, spontaneous excitatory postsynaptic current; spIPSC, spontaneous inhibitory postsynaptic current; spPSC, spontaneous postsynaptic current; THIP, 4,5,6,7-tetrahydroisoxazolo[5,4-c]pyridin-3-ol hydrochloride; TTX, tetrodotoxin.

- -

of synaptic GABA$_A$ receptors on A17s, which may play an important role in signal integration in these cells.

1 | INTRODUCTION

Neuronal inhibition is crucial for signal processing in microcircuits and networks of the central nervous system (CNS) and is exerted by inhibitory interneurons that constitute an extremely diverse group, morphologically, physiologically and biochemically. The connections between inhibitory interneurons and their targets are highly selective and precise, and there are multiple examples where an inhibitory interneuron targets discrete domains of the somato-dendritic region of a postsynaptic neuron, for example, as seen for the connections between presynaptic stellate and basket cells and postsynaptic Purkinje cells in the cerebellum (Palay & Chan-Palay, 1974). In addition to inhibition of excitatory neurons, inhibitory interneurons are themselves the targets of other inhibitory interneurons, and inhibition of inhibitory interneurons is a recurring motif in many neural circuits of the CNS (e.g. Cardin, 2018).

In the retina, amacrine cells constitute a very heterogeneous group of mostly inhibitory interneurons (Helmstaedter et al., 2013; MacNeil & Masland, 1998), with the most recent estimates (for mouse retina) suggesting more than 60 different types (Yan et al., 2020). The processes of amacrine cells are predominantly found in the inner plexiform layer, with synaptic inputs and outputs located along the same processes, often in close proximity to each other. Amacrine cells are thought to perform specific visual computations that modify the input–output transformations implemented by the excitatory connections between bipolar cells and ganglion cells (Franke et al., 2017; for reviews, see Diamond, 2017; Franke & Baden, 2017). In the retina, the functional role and importance of inhibitory input to amacrine cells are relatively unexplored, although there is extensive evidence from ultrastructural studies of amacrine inputs to specific types of amacrine cells (e.g. Park et al., 2020; Strettoi et al., 1992), including serial inhibitory synaptic connections between amacrine cells (e.g. Marc & Liu, 2000). Serial inhibitory synapses underscore the importance of 'tuning' inhibitory signalling, and it has to some extent been possible to explore such synaptic connections in physiological experiments (Eggers & Lukasiewicz, 2010; Zhang et al., 1997).

A particularly interesting example of an amacrine cell where the evidence for inhibitory synaptic inputs has been largely ignored is the mammalian A17 amacrine, a GABAergic wide-field amacrine that plays an important role in scotopic vision (Diamond, 2017; Diamond & Grimes, 2014). The A17 receives its excitatory input from rod bipolar axon terminals at dendritic varicosities in the middle and distal parts of the dendritic tree (Nelson & Kolb, 1985; Strettoi et al., 1990). The output is localized to the same varicosities and directed exclusively back onto the rod bipolar terminals, forming reciprocal inhibitory synapses (Chávez et al., 2006; Hartveit, 1999; Nelson & Kolb, 1985; Strettoi et al., 1990; Zhang et al., 2002). From ultrastructural investigations, however, there is also evidence for amacrine input to the A17, predominantly located at the proximal parts of the dendrites, both at varicosities and at intervaricosity segments (Nelson & Kolb, 1985). The identity of the amacrine input is unclear, but A17s express both GABA and glycine receptors (Majumdar et al., 2009; Menger & Wässle, 2000; Zhou et al., 2016), and there is evidence for an inhibitory component in the light response (Menger & Wässle, 2000). The consequent spatial segregation between excitatory (middle to distal) and inhibitory (proximal) inputs along A17 dendrites suggests that inhibition could be important for compartmentalization, perhaps by limiting signalling interaction between the major dendritic branches. For starburst amacrine cells, involved in generating retinal direction selectivity, there is strong evidence that synaptic inhibition is important for enhancing dendritic compartmentalization (Poleg-Polsky et al., 2018). If inhibition plays a similar role in A17s, it could suggest that signal processing in these cells is not intrinsically limited to microcircuits local to each dendritic varicosity (Grimes et al., 2010) and that spatial integration in these cells might occur over larger regions than currently thought (cf. Bloomfield, 1992; Nelson & Kolb, 1985; Völgyi et al., 2002; Zhang et al., 2002). As a first step to investigate the functional role of inhibitory inputs to A17 amacrine cells, we have investigated physiological and pharmacological properties of spontaneous inhibitory postsynaptic currents (spIPSCs) in these cells by performing whole-cell recordings in rat retinal slices. In addition, we used outside-out and nucleated patch recordings to characterize the biophysical and pharmacological properties of GABA$_A$ receptors expressed by A17 amacrine cells.

2 | MATERIALS AND METHODS

2.1 | Retinal slice preparation and visual targeting of neurons

General aspects of the methods have previously been described in detail (Gill et al., 2006; Veruki et al., 2003). The use of animals in this study was carried out under the approval of and in accordance with the Animal Laboratory Facility at the Faculty of Medicine at the University of Bergen (accredited by AAALAC International). Albino rats (Wistar HanTac; 4–7 weeks postnatal, both male and female) were deeply anaesthetized with isoflurane in oxygen and killed by cervical dislocation. Vertical retinal slices were cut by hand and visualized by using an upright microscope, either an Axioskop 2 FS (Zeiss) with a ×40 water immersion objective and infrared differential interference contrast (IR-DIC) videomicroscopy or a BX51WI (Olympus) with a ×40 or ×60 water immersion objective and IR-DIC or IR Dodt gradient contrast (IR-DGC) videomicroscopy (Luigs & Neumann, Ratingen, Germany).

2.2 | Solutions and drug application

The standard extracellular perfusing solution was continuously bubbled with 95% O_2–5% CO_2 and had the following composition (in mM): 125 NaCl, 25 $NaHCO_3$, 2.5 KCl, 2.5 $CaCl_2$, 1 $MgCl_2$, 10 glucose (pH 7.4). For whole-cell recordings, pipettes were filled with one of three solutions. The first solution, used for the majority of recordings of spontaneous postsynaptic currents (spPSCs), had the following composition (mM): 130 KCl, 8 NaCl, 10 HEPES, 1 $CaCl_2$, 5 EGTA, 4 MgATP, 2 N-(2,-6-dimethylphenylcarbamoylmethyl)triethylammonium bromide (QX-314; Tocris Bioscience) (pH adjusted to 7.3 with KOH). The second solution was used for experiments with acquisition of current–voltage (I-V) relationships and had the following composition (mM): 125 CsCl, 15 tetraethylammonium chloride (TEA-Cl), 8 NaCl, 10 HEPES, 1 $CaCl_2$, 5 EGTA, 4 MgATP. When combined with the standard extracellular solution, the calculated chloride equilibrium potential (E_{Cl}) was ~3 mV. The third solution was also used for experiments with acquisition of I-V relationships and had the following composition (mM): 125 $CsCH_3SO_3$, 15 TEA-Cl, 8 NaCl, 10 HEPES, 1 $CaCl_2$, 5 EGTA, 4 MgATP. When combined with the standard extracellular solution, the calculated E_{Cl} was ~−43 mV. For both Cs^+-based pipette solutions, pH was adjusted to 7.3 with CsOH. For outside-out and nucleated patch recordings, the pipettes were filled with (mM) 130 KCl, 8 NaCl, 10 HEPES, 1 $CaCl_2$, 5 EGTA, 4 MgATP and 2 QX-314 (pH adjusted to 7.3 with KOH). In some experiments (both whole-cell and nucleated patch recordings), QX-314 was omitted from the pipette solution. Alexa Fluor 594 (40 µM; Invitrogen/Thermo Fisher Scientific) was included in all pipette solutions and permitted visualization of the complete cellular morphology with wide-field fluorescence microscopy after both whole-cell and patch recordings.

For whole-cell recordings, drugs were added directly to the extracellular solution at the following concentrations (µM; supplier Tocris Bioscience, unless otherwise indicated): 0.3 strychnine (Research Biochemicals International; to block glycine receptors), 3 or 10 SR95531 (to block $GABA_A$ receptors), 10 6-cyano-7-nitroquinoxaline-2,3-dione (CNQX; Tocris Bioscience or Hello Bio; to block non-NMDA receptors), 20 (RS)-3-(2-carboxypiperazin-4-yl)-propyl-1-phosphonic acid (CPP; Tocris Bioscience or Hello Bio; to block NMDA receptors), 0.3 tetrodotoxin (TTX; to block voltage-gated Na^+ channels). To modulate $GABA_A$ receptors, $ZnCl_2$ (10 µM, 100 µM, 500 µM or 1 mM; Sigma) or zolpidem (100 nM or 1 µM; Synthélabo Recherche) were added directly to the bath solution. Solutions were either made up freshly for each experiment or were prepared from aliquots stored at −20°C and diluted to the final concentration on the day of the experiment.

2.3 | Ultra-fast drug application

Ultra-fast drug application was performed according to the general description of Jonas (1995) and as detailed in Veruki et al. (2003) and Hartveit et al. (2018). Drugs were applied from a theta-tube application pipette with two separate barrels (septum thickness ~117 µm, final tip diameter ~300 µm; Hilgenberg, Malsfeld, Germany). The pipette tip with the patch (outside-out or nucleated) was positioned near the interface between the control solution and the agonist-containing solution continuously flowing out of each barrel, about 100 µm away from the tip of the application pipette. Concentration jumps of agonist to the patch were performed by rapidly moving the application pipette and thus the interface between the two solutions. The solution exchange time was measured as previously described (Veruki et al., 2003). Under optimal conditions, the 20%–80% rise time of the solution exchange ranged from 150 to 400 µs. For ultra-fast application, GABA was dissolved in a HEPES-buffered solution containing (mM) 145 NaCl, 2.5 KCl, 2.5 $CaCl_2$, 1 $MgCl_2$, 5 hemiNa-Hepes and 10 glucose (pH adjusted to 7.4 with HCl). Agonist pulses were applied at intervals of 30–40 s. The second barrel of the theta-tube application pipette ('control') was filled with the same HEPES-buffered solution without agonist. Alternatively, it was

filled with the HEPES-buffered solution containing one of the following chemicals to potentially modulate or block $GABA_A$ receptors: $ZnCl_2$ (10, 100 or 500 μM), zolpidem (100 nM or 1 μM), 4,5,6,7-tetrahydroisoxazolo [5,4-*c*]pyridin-3-ol hydrochloride (THIP; 1, 5 or 10 μM) or SR95531 (3 μM). When we switched between solutions with different composition flowing into the second barrel, full exchange required 85–100 s.

2.4 | Electrophysiological recording and data acquisition

Patch pipettes were pulled from thick-walled borosilicate glass (outer diameter, 1.5 mm; inner diameter, 0.86 mm; Sutter Instrument) to obtain an open-tip resistance that ranged from 5 to 7 MΩ when filled with intracellular solution. Whole-cell voltage-clamp recordings were performed with an EPC9-dual or EPC10-dual amplifier and controlled with Patchmaster software (HEKA Elektronik, Lambrecht/Pfalz, Germany). After establishing a GΩ seal, currents caused by the recording electrode capacitance were automatically measured and neutralized by the amplifier (fast capacitive current; 'C_{fast}' function in Patchmaster). After breaking into the cell, currents caused by the cell membrane capacitance were partially neutralized by the amplifier (slow capacitive current; 'C_{slow}' function in Patchmaster). For whole-cell recordings, the series resistance (R_s) was not compensated, but was monitored throughout the recording (at intervals of 1 min for most experiments) by applying a series of 20-mV hyperpolarizing voltage pulses (20-ms duration) after transiently disabling the C_{slow} neutralization circuitry of the amplifier and switching the stimulus filter to 2 μs. For offline analysis of R_s, we fitted the decay phase of the charging transients (following onset of the voltage pulse) with a double-exponential function (Fitmaster software; HEKA Elektronik) and calculated R_s from the amplitude of the voltage pulse and the peak current amplitude extrapolated to the onset of the pulse. Cells with $R_s > 40$ MΩ or holding current (I_{hold}) more negative than -50 pA (at a holding potential of -70 mV) were not included in the final material.

Outside-out and nucleated patch recordings were established by slowly withdrawing the recording pipette after establishing the whole-cell recording configuration. To obtain nucleated patches, continuous light suction (∼50 mbar) was applied to the pipette while it was withdrawn. When an outside-out or nucleated patch was successfully isolated, the reduced membrane capacitance resulted in capacitive current transients of the opposite polarity that were cancelled by readjustment of the C_{slow} neutralization circuitry. Signals were low-pass filtered (analog three- and four-pole Bessel filters in series) with a corner frequency (-3 dB) typically at 1/5 of the inverse of the sampling interval (20 or 50 μs depending on the experiment). All recordings were carried out at room temperature (22–25°C). The data acquisition software (Patchmaster) corrected all holding potentials for liquid junction potentials online. Theoretical liquid junction potentials were calculated with JPCalcW (Molecular Devices, Sunnyvale, CA, USA).

For most whole-cell recordings, the input resistance (R_N) was estimated offline from the resistive (steady-state) current response (averaged from 100 repetitions) evoked by a 20-mV hyperpolarizing voltage pulse from a holding potential (V_{hold}) of -70 mV (20-ms duration) by dividing the voltage pulse amplitude by the evoked current (averaged from a 15- to 19-ms interval after onset of the voltage pulse).

2.5 | Wide-field fluorescence microscopy

All cells (for whole-cell and patch recordings) were imaged with wide-field fluorescence microscopy after recording to confirm the identity of the cell by verifying the full morphology. The morphology of each dye-filled neuron and its processes and the relationship between the branching pattern and the strata of the inner plexiform layer were documented with a hand-drawn sketch. In addition, for some cells, we acquired image stacks using a digital CCD camera (CoolSnap ES; Photometrics/Roper Scientific) controlled by μManager software (www.micro-manager.org) running under Windows XP. During image acquisition, exposure to UV light was controlled by an electronic shutter (Uniblitz VCM-D1, Vincent Associates, Rochester, NY, USA), thereby minimizing the total exposure time. After acquisition, Huygens (Scientific Volume Imaging, Hilversum, The Netherlands) was used to remove noise and reassign out-of-focus light by deconvolution with a theoretical point-spread function (CMLE method; for details, see Zandt et al., 2017). Maximum intensity projections were generated in Huygens that also enabled adjustment of contrast, brightness and gamma (over the entire image).

2.6 | General data analysis

Data were analysed with Fitmaster, IGOR Pro (WaveMetrics, Lake Oswego, OR, USA), Excel, AxoGraph (AxoGraph Scientific, Sydney, Australia), MiniAnalysis (Synaptosoft, Decatur, GA, USA) and GraphPad Prism 6.0 (GraphPad Software, La Jolla, CA, USA). All curve fitting was done with IGOR Pro.

For detection of spIPSCs with MiniAnalysis, the threshold was set between 6 and 8 pA, depending on the noise level. All detected events were confirmed by eye. For kinetic analysis, we included only well-separated, monophasic spIPSCs (interevent interval ≥ 30 ms) that appeared to rise in a monotonic fashion to a peak followed by an exponential decay. To quantify the reduction of spIPSC amplitude evoked by Zn^{2+}, we used the method of largest amplitude count matching (Stell & Mody, 2002).

Before averaging, individual spIPSCs and patch responses were aligned at the point of steepest rise. The decay time course of individual and averaged spIPSCs and patch responses was estimated by curve fitting with exponential functions. For single-exponential functions, we used the function

$$I(t) = A \times e^{(-t/\tau)} + I_{ss} \qquad (1)$$

where $I(t)$ is the current as a function of time, A is the amplitude at time 0, τ is the time constant and I_{ss} is the steady-state current amplitude (typically zero). For double-exponential functions, we used the function

$$I(t) = A_1 \times e^{(-t/\tau_1)} + A_2 \times e^{(-t/\tau_2)} + I_{ss} \qquad (2)$$

where $I(t)$ is the current as a function of time, A_1 and A_2 are the amplitudes at time 0 of the first and second exponential components, τ_1 and τ_2 are the time constants of the first (fast) and second (slow) exponential components and I_{ss} is the steady-state current amplitude. For triple-exponential functions, a third component $A_3 \times e^{(-t/\tau_3)}$ was added to Equation 2. Fitting was generally started 50–500 μs after the peak amplitude of the averaged response. For double- and triple-exponential functions, the amplitude contribution of a given component A_x (A_1, A_2 or A_3) was calculated as $100\% \times A_x/(A_1 + A_2)$ or $100\% \times A_x/(A_1 + A_2 + A_3)$, respectively. As the relative amplitude of the exponential components depends on the definition of time 0, we defined the start of the response as the point in time at which the current rose from the baseline noise (as determined by eye). For double- and triple-exponential fits, a weighted time constant (τ_w) was calculated as the sum of the individual time constants multiplied by the relative amplitude contribution of the corresponding amplitude.

For acquisition of I-V relationships of spIPSCs, we recorded spIPSCs at a series of holding potentials ranging from −80 to +40 mV (increments of 20 mV). The potential was stepped to a new constant value before the start of sampling for 10 s to allow the membrane current to

relax to a plateau level. For each holding potential, spIPSCs from 50- to 200-s sampling periods were averaged as above. Data points of I-V relationships were fitted with a straight line or a third-order polynomial function. Reversal potentials (E_{rev}) were determined from the intersection of the fitted line with the abscissa. To measure the peak amplitude of GABA-evoked currents from nucleated and outside-out patch recordings, responses to GABA were baseline subtracted and averaged (typically from 5 to 30 repetitions). For longer lasting GABA applications, the steady-state response was measured as the average current of a 100-ms-long period at the end of the application. For illustration purposes, most raw data records were low-pass filtered (−3 dB; digital non-lagging Gaussian filter at 1–2 kHz). Unless otherwise noted, the current traces shown in the figures represent individual traces.

2.7 | Non-stationary noise analysis

For peak-scaled non-stationary noise analysis of spIPSCs (for review and details, see Hartveit & Veruki, 2007), only well-separated (interevent interval ≥ 30 ms), monophasic and monotonically rising events were included. The number of events included in the analysis for each cell ranged from 35 to 141. The ensemble variance was calculated from the difference waveforms obtained by subtracting the ensemble mean waveform (i.e. the average of all spIPSCs) from each spIPSC. To correct for quantal variability, the peak of the ensemble mean current response waveform was scaled to the response value at the corresponding point in time of each individual spIPSC before subtraction to generate the difference waveforms. The ensemble mean IPSC was binned, and variance versus mean curves were plotted for the decay phase of the IPSC (i.e. the interval between the peak response and the end of the decay phase) and fitted with the parabolic function:

$$\sigma^2(I) = iI - I^2/N + \sigma_b^2 \qquad (3)$$

where $\sigma^2(I)$ is the variance as a function of mean current, i is the apparent single-channel current, N is the average number of open channels at the spIPSC peak and σ_b^2 is the variance of the background noise. The apparent single-channel chord conductance (γ) was then calculated as:

$$\gamma = i/(V_m - E_{rev}) \qquad (4)$$

from the known holding potential (V_m) and assuming $E_{rev} = 0$ mV for recordings where E_{Cl} was ~0 mV.

For non-stationary noise analysis of patch responses, the ensemble variance was calculated by a pairwise subtraction of successive responses to minimize errors due to rundown of the responses (Heinemann & Conti, 1992). The number of events included in the analysis for each patch ranged from 9 to 49. As for the spIPSCs, the ensemble variance was plotted against the ensemble mean current and fitted with Equation 3. In this case, i, I and σ_b^2 have the same meaning as for the analysis of spIPSCs, but N corresponds to the number of available channels in the patch. The open probability (P_o) was calculated using the equation

$$P_o = I/iN \qquad (5)$$

3 | STATISTICAL ANALYSIS

Data are presented as means $\pm$ SD (n = number of cells, patches or responses) with ranges either displayed by individual data points in bar graphs or stated explicitly. Percentages are calculated as percentage of control. Statistical analyses with comparisons between or within groups were performed using either Student's two-tailed t-test (paired or unpaired), or the Kolmogorov–Smirnov test as indicated, using either GraphPad Prism or IGOR Pro. Differences were considered statistically significant at the $p \leq 0.05$ level.

4 | RESULTS

4.1 | Targeting and identification of A17 amacrine cells in rat retinal slices

The cell bodies of A17 amacrine cells can be readily targeted in the retinal slice based on their characteristic dome-like shape with a flat base at the border between the inner nuclear layer and the inner plexiform layer (Figure 1a; e.g. Beltrán-Matas et al., 2021; Castilho et al., 2015; Eggers & Lukasiewicz, 2006; Elgueta et al., 2018; Grimes et al., 2009, 2010, 2014; Menger & Wässle, 2000; Veruki et al., 2019; Zhou et al., 2016). To verify that a given recording (whole-cell, outside-out and nucleated patch) was from an A17 amacrine cell, the full morphology of the recorded cell and its dendritic tree was examined with fluorescence microscopy after diffusion of dye (Alexa 594) from the recording pipette. A17 amacrine cells have long, thin processes that carry distinct varicosities and extend several hundred μm laterally before

terminating in stratum 5 (S5) of the inner plexiform layer (Figure 1b). For this study, we have included results and analyses for a total of 120 A17 amacrine cells, including 57 whole-cell, 40 outside-out patch and 23 nucleated patch recordings. We never observed dye coupling of A17 amacrines, but for 55 whole-cell recordings, we estimated R_N (see Section 2), which was 379 ± 455 MΩ (range 98 MΩ to 2.8 GΩ; Figure 1c). This is similar to the values reported by Elgueta et al. (2018), and we therefore assume that the large majority of our cells were electrically coupled (cf. Elgueta et al., 2018; Grimes et al., 2014).

4.2 | A17 amacrine cells display inhibitory spPSCs

As a first step to characterize the inhibitory input received by A17 amacrines, we performed whole-cell recordings of spPSCs at $V_{hold} = -70$ mV ($E_{Cl} \sim 0$ mV). To block glutamatergic, excitatory spPSCs (spEPSCs) and the potential influence of presynaptic action potential firing, we added CNQX and TTX to the bath solution. In this condition, cells identified as A17 amacrine cells displayed spPSCs that appeared as inward currents and occurred at a relatively low, irregular frequency. For the cell illustrated in Figure 1d, the frequency (measured over a 3-min period) was $\sim$1 Hz. An interevent interval histogram, constructed from all spPSCs recorded during the 3-min period, was well fitted by a single-exponential function ($\tau = 0.9$ s), suggesting a random occurrence of the spPSCs (Figure 1e). For a total of 10 cells recorded in this condition, the average frequency was 1.4 ± 2.0 Hz (range 0.16–7.0 Hz). Nine of these cells had a sufficient number of spPSCs to construct interevent interval histograms. For eight of the nine cells, the interevent interval histogram could be well fitted by a single-exponential function ($\tau = 1.3 \pm 1.1$ s; range 0.14–3.1 s), consistent with a random occurrence of spPSCs. For one cell, the interevent interval histogram was better fitted with a double-exponential function, suggesting a tendency towards temporal clustering of the spPSCs. The amplitude histograms were mostly skewed towards larger values, as is typically seen for spPSCs in CNS neurons (e.g. Nusser et al., 1997). For the cell illustrated in Figure 1d,e, the mode of the amplitude histogram was 7 pA, and the mean was 10.5 pA (range 6.0–31.2 pA; Figure 1f). For the 10 cells recorded in this condition, the average of the mode amplitude was 9.2 ± 3.0 pA (range 6–16 pA), and the average of the mean amplitude was 18.9 ± 10.1 pA (range 9.2–43.3 pA).
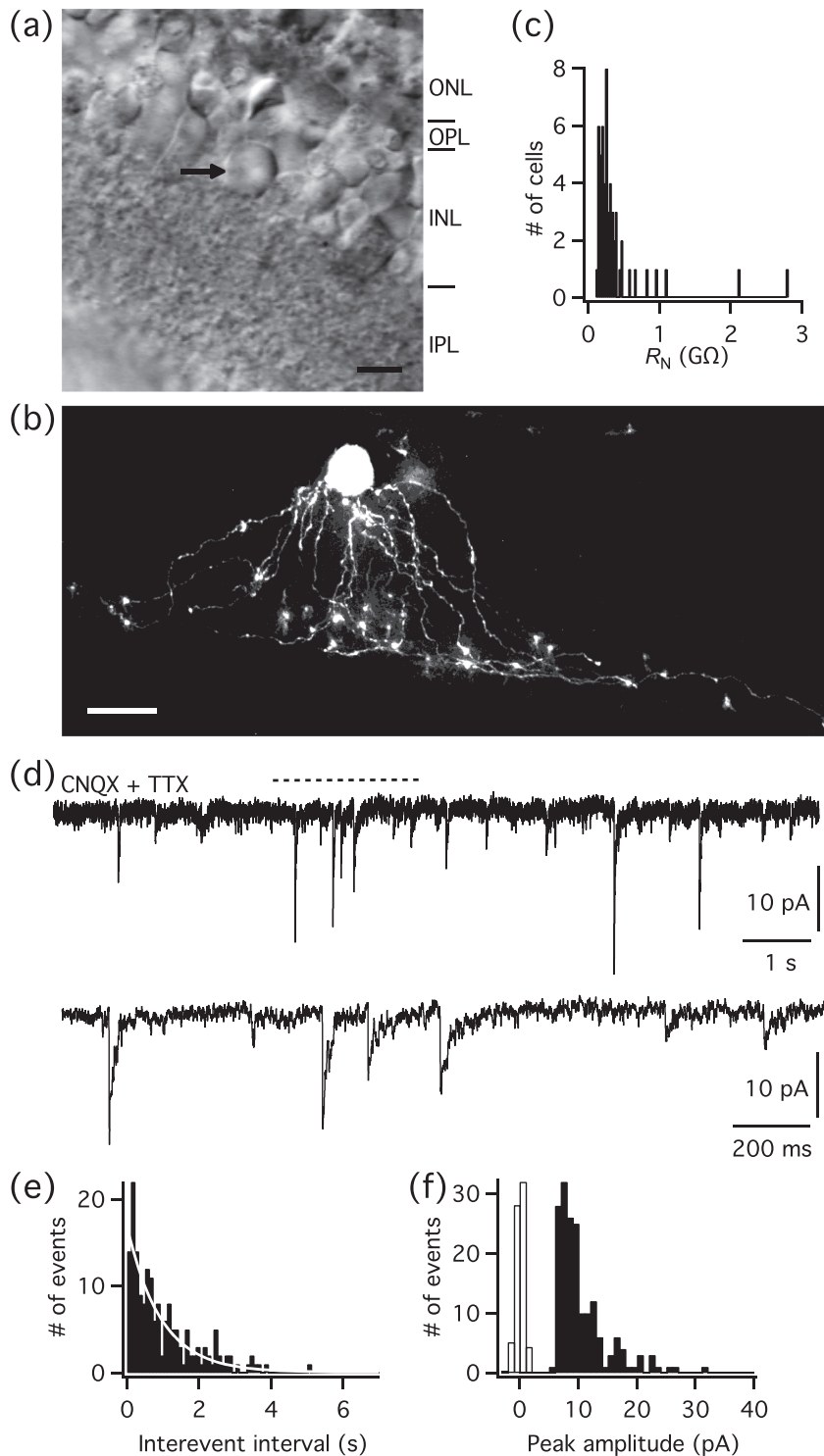
FIGURE 1 A17 amacrine cells in the rat retinal slice preparation. (a) Infrared differential interference contrast (IR-DIC) videomicrograph of an A17 amacrine cell (arrow) in a retinal slice. The retinal layers are marked by horizontal lines and by abbreviations (right: ONL, outer nuclear layer; OPL, outer plexiform layer; INL, inner nuclear layer; IPL, inner plexiform layer). Scale bar, 10 μm. (b) Wide-field fluorescence image of an A17 amacrine cell filled with Alexa 594 via the patch pipette (maximum intensity projection of image stack after deconvolution). Scale bar, 20 μm. (c) Frequency histogram showing distribution of values for input resistance (R_N) for A17 amacrine cells in the whole-cell configuration ($n = 55$ cells). Bin width 27 MΩ. (d) Spontaneous postsynaptic currents (spPSCs) in a whole-cell voltage-clamp recording of an A17 amacrine cell with 10 μM CNQX and 300 nM TTX in the extracellular solution. Here and later, $V_{hold} = -70$ mV and $E_{Cl} \sim 0$ mV (unless otherwise noted). Activity is displayed at both a slow (upper panel) and a fast (lower panel) time scale. Broken line above upper panel indicates the duration of the period displayed in the lower panel. (e) Interevent interval histogram of spPSCs recorded during 180 s ($n = 176$ events; same cell as in (d)); bin width 100 ms; single-exponential fit indicated by white line ($\tau = 940$ ms). Here and in (f), each histogram displays all events. (f) Amplitude distribution of spPSCs recorded in CNQX and TTX; peak (mode) at 7 pA; notice skew towards larger amplitudes; bin width 1 pA. The noise distribution is shown as an unfilled histogram (peak scaled to the peak of the spPSC amplitude distribution)

4.3 | Spontaneous IPSCs in A17 amacrines are mediated by GABA_A receptors

When spPSCs in A17 amacrines appeared as inward currents in recordings with $V_{hold} = -70$ mV, $E_{Cl} \sim 0$ mV and pharmacological block of non-NMDA-type glutamate receptors, it suggested that these were inhibitory spPSCs (spIPSCs), most likely mediated by chloride channels integral to GABA and/or glycine receptors. To further investigate the functional identity of the spIPSCs, we examined the effect of antagonists selective for either GABA_A or glycine receptors. We first recorded spIPSCs in a control condition (with CNQX and TTX in the bath solution) and then tested for the potential involvement of glycine receptors by adding the glycine receptor

antagonist strychnine at a concentration of 300 nM. At this concentration, strychnine is expected to be selective for glycine receptors, with no block of GABA$_A$ receptors (Lewis & Faber, 1993). For the cell illustrated in Figure 2a, there was essentially no change in frequency of the spIPSCs with application of strychnine. As measured over 3-min periods, the frequency of spIPSCs was 0.9 Hz in the control condition and 1.0 Hz in the presence of strychnine. For a total of six A17 amacrine cells, no significant change in frequency of spIPSCs occurred following addition of strychnine, with an average frequency of spIPSCs of 1.8 ± 2.6 Hz in control (range 0.16–7.0 Hz), compared with an average frequency of 1.5 ± 1.8 Hz in the presence of strychnine (range 0.19–5.1 Hz; $p = 0.4427$, paired t-test; Figure 2b). This could suggest that the sources of GABAergic input to the A17s do not receive much glycinergic input, at least under our recording conditions. We also investigated potential changes in amplitude by calculating the cumulative amplitude of all events in the same epochs that were used to estimate the frequency. In control, the average cumulative amplitude was 6.6 ± 7.9 nA (range 0.46–21 nA), which was not significantly different from the average cumulative amplitude of 4.8 ± 4.4 nA (range 0.37–12 nA) obtained after the addition of strychnine ($p = 0.2458$, paired t-test; Figure 2c). Taken together, this suggested that the spIPSCs recorded in A17 amacrines were unlikely to be mediated by glycine receptors.

We next recorded spIPSCs in the presence of strychnine, CNQX and TTX and examined the potential involvement of GABA$_A$ receptors by adding the GABA$_A$ receptor antagonist SR95531 (3 μM) to the bath solution. At this concentration, SR95531 is not expected to have a significant effect on glycine-mediated synaptic currents (Protti et al., 1997). For the cell illustrated in Figure 2d, SR95531 completely blocked the spIPSCs, and the block was fully reversed after washout. For a total of seven cells (with an average frequency of spIPSCs in the control condition of 1.6 ± 1.4 Hz), SR95531 completely and reversibly blocked the spIPSCs (Figure 2e). This strongly suggested that all the observed spIPSCs were mediated by GABA$_A$ receptors. This conclusion was strengthened by the observation that SR95531 completely (and reversibly) blocked the spIPSCs recorded in the absence of strychnine ($n = 3$ cells; Figure 2f,g).

Earlier work in our laboratory found that A17 amacrine cells express NMDA receptors, seemingly only with an extrasynaptic location (Veruki et al., 2019; Zhou et al., 2016). Thus, for some experiments, we included the NMDA receptor antagonist CPP in the extracellular solution. To examine if adding CPP influenced the GABAergic spIPSCs, we first recorded spIPSCs in a control condition (with CNQX and strychnine in the bath), followed by the addition of CPP (20 μM). For the cell

illustrated in Figure 2h, the frequency of GABA$_A$ receptor-mediated spIPSCs was 1.4 Hz in control and 0.8 Hz in CPP. There was no change in the amplitude of the spIPSCs, as observed by comparing the cumulative probability density distributions for peak amplitude in the two conditions (Figure 2i; $p = 0.615$, Kolmogorov–Smirnov test). Similar results were observed for a total of four A17s, with a significant decrease in the frequency of spIPSCs from control (9.0 ± 9.3 Hz, range 1.4–22 Hz) to CPP (6.2 ± 8.4 Hz, range 0.82–19 Hz; $p = 0.0346$, paired t-test; Figure 2j). For three of these cells, there was no significant difference in spIPSC amplitude distribution between control and CPP ($p > 0.17$, Kolmogorov–Smirnov test). In contrast, for the fourth cell, despite no change in the average spIPSC amplitude between control (17.6 ± 8.0 pA, $n = 652$ events) and CPP (16.9 ± 8.8 pA, $n = 357$ events), there was a significant difference between the corresponding amplitude distributions ($p = 0.0025$, Kolmogorov–Smirnov test). These results suggested that CPP has no direct effect on GABAergic spIPSCs of A17 amacrine cells. It is likely, however, that (some) GABAergic neurons presynaptic to the A17s express NMDA-type glutamate receptors that contribute to the excitatory drive. For most of the experiments included in the current study, CPP was not included in the bath solution, and we explicitly state when CPP was added.

In conclusion, our results suggest that the spIPSCs recorded in A17 amacrines in rat retinal slices are mediated by GABA$_A$ receptors. This contrasts with results for displaced A17 amacrine cells in mouse retina, where the spIPSCs were glycinergic (Majumdar et al., 2009). It is possible that under other recording conditions, for example, states of light adaptation, glycinergic spIPSCs might be observed also in rat A17s (with cell bodies located in the inner nuclear layer). To avoid any confounding effects caused by the potential occurrence of glycinergic spIPSCs, we included strychnine at a concentration of 300 nM in all subsequent recordings of spIPSCs. At this concentration, we consider it unlikely that strychnine will block GABA$_A$ receptor-mediated synaptic currents of A17 amacrine cells (cf. Lewis & Faber, 1993).

4.4 | Kinetic properties of GABAergic spIPSCs in A17 amacrine cells

To study the kinetic properties of the GABA$_A$ receptor-mediated spIPSCs, recordings were performed in the presence of CNQX, strychnine and TTX. We limited the analysis to A17 amacrine cells with low (<40 MΩ) and stable R_s (average 25 ± 5 MΩ, range 19–35 MΩ) and I_{hold} less negative than −50 pA (average −18 ± 22 pA, range −50 to +10 pA; $V_{hold} = -70$ mV; $n = 10$ cells). For this analysis,
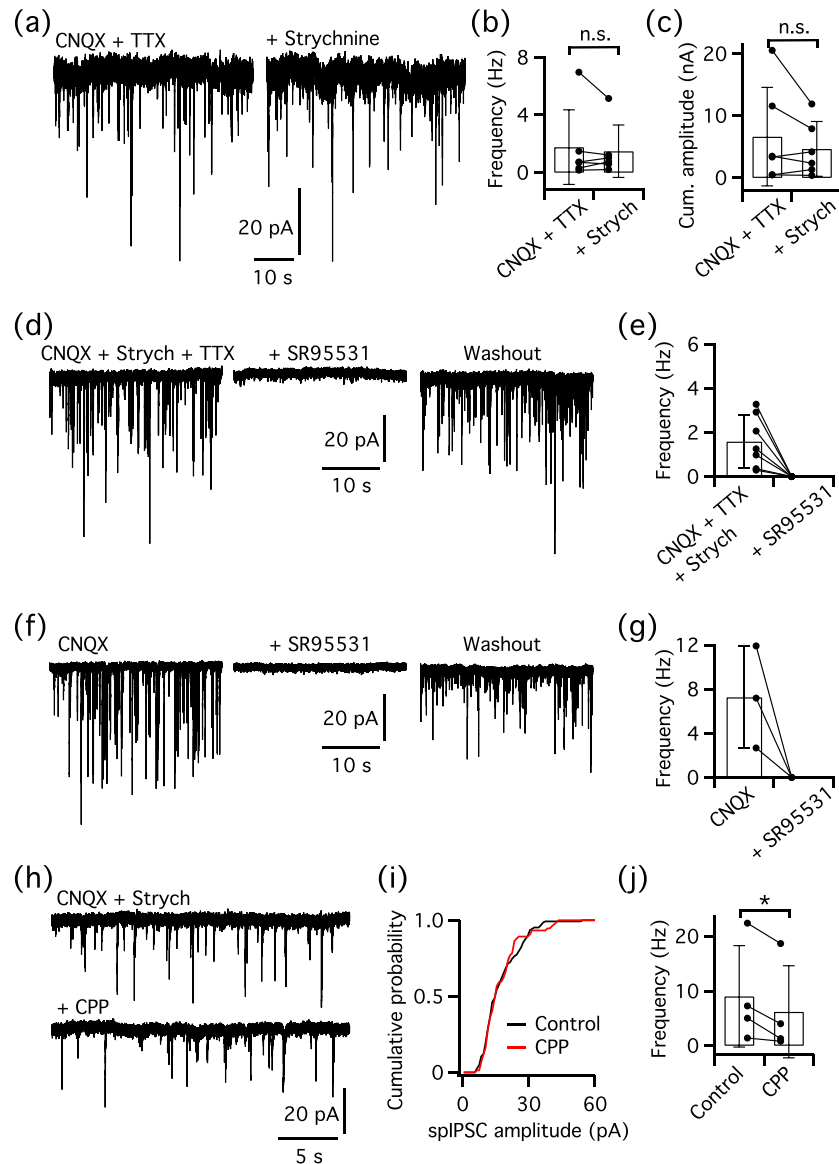
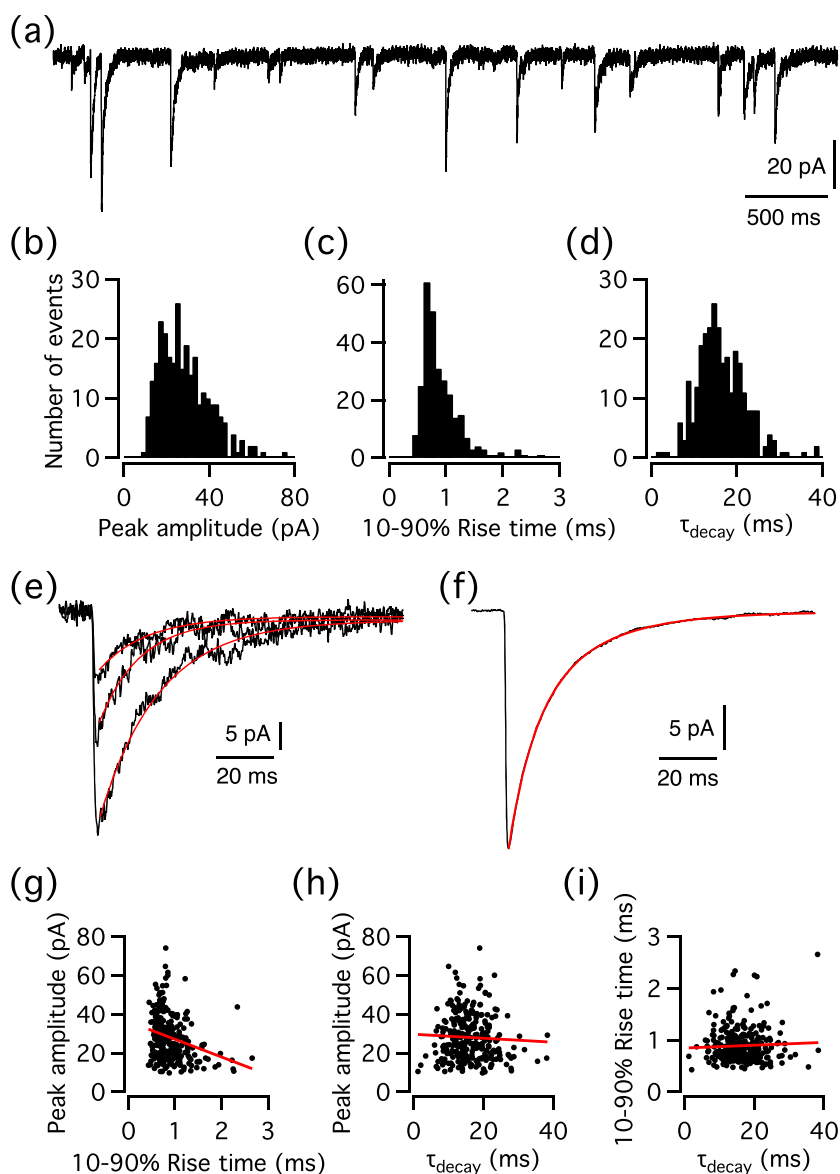**FIGURE 2** Properties of GABA$_A$ receptor-mediated spontaneous IPSCs (spIPSCs) in A17 amacrine cells. (a) spIPSCs (recorded in the presence of 10 μM CNQX and 300 nM TTX) are not blocked by adding 300 nM strychnine to the bath solution. (b) Frequency of spIPSCs (here and later, bars represent mean ± SD) in the presence of CNQX + TTX and in the presence of CNQX + TTX + strychnine ($n = 6$ cells). Here and later, data points for the same cell (or patch) are represented by circles connected by lines and the results from statistical comparisons between averages are indicated by n.s. (no significant difference; $p > 0.05$) and a single asterisk (statistically significant difference; $p < 0.05$), except when a pharmacological agent completely blocked the synaptic activity. (c) Cumulative peak amplitude of spIPSCs occurring over a 180-s period in the presence of CNQX + TTX and in the presence of CNQX + TTX + strychnine ($n = 6$ cells). (d) spIPSCs (recorded in the presence of 10 μM CNQX, 300 nM TTX and 300 nM strychnine) are reversibly blocked by adding 3 μM SR95531 to the bath solution. (e) Frequency of spIPSCs in the presence of CNQX + TTX + strychnine and in the presence of CNQX + TTX + strychnine + SR95531 ($n = 7$ cells). (f) spIPSCs (recorded in the presence of 10 μM CNQX) are reversibly blocked by adding 3 μM SR95531 to the bath solution. (g) Frequency of spIPSCs in the presence of CNQX and in the presence of CNQX + SR95531 ($n = 3$ cells). (h) spIPSCs (recorded in the presence of 10 μM CNQX and 300 nM strychnine) are not blocked by adding 20 μM CPP to the bath solution. (i) Adding CPP to the bath solution does not change the peak amplitude distribution of spIPSCs in an A17 amacrine cell. The graph shows the cumulative probability density (relative frequency) distributions of peak amplitude for the population of events recorded in the control condition (CNQX + strychnine; black line; $n = 123$ events) and after adding CPP (red line; $n = 74$ events). (j) Frequency of spIPSCs in the presence of CNQX + strychnine and in the presence of CNQX + strychnine + CPP ($n = 4$ cells)

we selected well-separated events (interevent interval ≥ 30 ms) with monophasic, monotonically rising waveforms recorded over a period of 3 min. For each cell, we measured kinetic and amplitude properties for all individual events and for the ensemble average. A short epoch of a recording from a representative cell is illustrated in Figure 3a. The peak amplitude of the individual spIPSCs varied between 9.8 and 74 pA, with an average of 28 ± 12 pA (Figure 3b; $n = 280$ events). The 10%–90% rise time of the individual spIPSCs ranged from 431 to 2660 μs, with an average of 893 ± 342 μs (Figure 3c). When the decay was fitted with a single-exponential function, τ_{decay} varied from 1.3 to 38.4 ms, with an average of 16.2 ± 5.7 ms (Figure 3d). For individual spIPSCs, the decay phase was reasonably well fitted with a single-exponential function, as illustrated for three events in Figure 3e. For the average waveform of the ensemble of

spIPSCs, however, a good fit of the decay required a double-exponential function, with $\tau_{fast} = 8.2$ ms, $\tau_{slow} = 24$ ms and amplitude contributions of 52% and 48%, respectively (Figure 3f). The weighted decay time constant (τ_w) was 16 ms.

For all 10 A17 amacrine cells, we analysed the kinetic properties for spIPSCs recorded during a 3- to 4-min period. The number of individual spIPSCs that satisfied the criteria described above ranged from 46 to 280. For the average waveforms of the spIPSC ensembles, the population average of the peak amplitude was 21.6 ± 7.4 pA (range 14.2–35.9 pA), and the population average of the 10%–90% rise time was 738 ± 83 μs (range 634–918 μs). Because we wanted to compare these properties with those obtained from patches (see below) and from other studies, we also measured the 20%–80% rise time (average 473 ± 49 μs, range 410–575 μs). A good fit of the decay

FIGURE 3 Kinetics of GABA$_A$ receptor-mediated spIPSCs in A17 amacrine cells. (a) spIPSCs in a whole-cell voltage-clamp recording of an A17 amacrine cell with 10 μM CNQX, 300 nM strychnine and 300 nM TTX in the extracellular solution. Data from the same cell in (a)–(i). (b) Amplitude distribution of spIPSCs ($n = 280$ events, temporally well separated from each other; same events in (b)–(d)); bin width 1 pA. (c) Distribution of 10%–90% rise time for spIPSCs; bin width 0.1 ms. (d) Distribution of τ_{decay} for spIPSCs (single-exponential fit); bin width 1 ms. (e) Three overlaid spIPSCs (black lines), aligned at their onset. A single-exponential fit (red line) has been overlaid on the decay phase of each spIPSC (τ_{decay} was 16.6 ms for the smallest event, 14.1 ms for the medium size event and 20.7 ms for the largest event). (f) Average waveform of all spIPSCs ($n = 280$; black line) overlaid with a double-exponential fit (red line). (g) Relation between spIPSC peak amplitude and 10%–90% rise time. (h) Relation between spIPSC peak amplitude and τ_{decay}. (i) Relation between 10%–90% rise time and τ_{decay}

time course of the ensemble average IPSCs consistently required a double-exponential function. The population average τ_{fast} was 4.5 ± 2.4 ms (range 2.0–8.2 ms; $39 \pm 16\%$ amplitude contribution), and the population average τ_{slow} was 21.5 ± 3.8 ms (range 15.6–25.9 ms; $61 \pm 16\%$ amplitude contribution). The weighted decay time constant (τ_w) was 14.8 ± 3.0 ms (range 12–22 ms).

We also analysed the relationships between peak amplitude, 10%–90% rise time and τ_{decay} (determined by a single-exponential fit) for the ensemble of individual spIPSCs for each of the 10 cells. For the cell illustrated in Figure 3, there was a negative correlation between peak amplitude and 10%–90% rise time, that is, the larger spIPSCs displayed smaller values for rise time (Spearman's $R = -0.27$, $p = 6.4 \times 10^{-6}$; Figure 3g). In contrast, there was no correlation between peak amplitude and τ_{decay} (Spearman's $R = -0.04$, $p = 0.4642$; Figure 3h) or between 10%–90% rise time and τ_{decay} (Spearman's $R = -0.01$, $p = 0.8939$; Figure 3i).

A negative correlation between peak amplitude and 10%–90% rise time was observed for all 10 cells analysed. For five of the 10 cells, the negative correlation was statistically significant (Spearman's R varied between -0.46 and -0.19; $p < 0.0226$; $n = 5$). Whereas the smallest events spanned the range of rise times, the largest events typically had faster rise times (as in Figure 3g). This could suggest that the spIPSC waveforms were influenced by differential electrotonic filtering in the dendritic tree, with the largest events being less heavily filtered, most likely because they are generated closer to the soma. Events generated further from the soma would be more heavily filtered, resulting in smaller amplitudes and longer rise times (Barberis et al., 2004; Gardner et al., 1999). There was no correlation between peak amplitude and τ_{decay} for nine of the 10 cells. For one cell, there was a positive correlation, that is, the largest events had the longest decay times (Spearman's $R = 0.29$; $p = 0.0054$). Finally, there was no correlation between 10%–90% rise time and τ_{decay} for the 10 cells. In summary, these results suggest that for each cell, the recorded GABAergic spIPSCs are likely to be generated at different distances from the soma and therefore may undergo differential electrotonic filtering. Potentially, the recorded spIPSCs could also be generated by different input sources, that is, from different types of GABAergic amacrine cells presynaptic to the A17 amacrines.

4.5 | Reversal potential and voltage dependence of GABA$_A$ receptor-mediated spIPSCs in A17 amacrine cells

To further characterize the GABAergic spIPSCs in A17 amacrines, we used whole-cell voltage-clamp recordings (with a Cs^+-based intracellular solution) to examine their E_{rev} and voltage dependence. By using intracellular solutions with two different chloride concentrations, we obtained values for E_{Cl} of ~ 3 and ~ -43 mV, respectively. The bath solution contained CNQX, strychnine and TTX. For the cell illustrated in Figure 4a, the recording was performed with high intracellular chloride concentration (E_{Cl} ~ 3 mV), and we observed spIPSCs at all holding potentials, except at 0 mV. At negative potentials, the spIPSCs appeared as inward currents, and at positive potentials, they appeared as outward currents. When we displayed the averaged IPSCs obtained at each potential, it could be observed that the decay was faster at negative than at positive potentials (Figure 4b). To construct an I-V relationship, we plotted the peak amplitude of each averaged IPSC (Figure 4b; ●) against the membrane potential (Figure 4c; ●). The I-V relationship was relatively linear in the region around the reversal potential but displayed some rectification at more negative membrane potentials (Figure 4c). Between -40 and $+40$ mV, the data points could be well fitted with a straight line (Figure 4c). For seven cells analysed in this way (line fit between -40 and $+40$ mV), the average E_{rev} was -1.4 ± 4.9 mV (range -8.3 to 7.2 mV). Because the decay time course of the IPSCs was voltage dependent (Figure 4a,b), we also constructed I-V relationships by measuring the current ~ 25 ms after the peak amplitude (Figure 4b; ○). In this situation, the I-V relationship displayed clear outward rectification (data points were fitted with a third-order polynomial function for illustration purposes; Figure 4c; ○). We also analysed the voltage-dependent decay time course by fitting the decay of the averaged IPSCs at -80 and $+40$ mV with a double-exponential function. At $+40$ mV, the average τ_w was 50 ± 18 ms (range 32–72 ms), significantly slower than τ_w at -80 mV (12.2 ± 2.6 ms, range 9.4–16 ms; $p = 0.0019$, paired t-test; $n = 7$ cells; Figure 4d).

For the second set of experiments, we used an intracellular solution with low chloride concentration (E_{Cl} ~ -43 mV). In this condition, we observed spIPSCs at all holding potentials, except at -40 mV (Figure 4e). The spIPSCs appeared as either inward or outward currents (with increasing amplitudes) at potentials more negative and more positive to -40 mV, respectively. The I-V relationship constructed by plotting the peak amplitude of each averaged IPSC against the membrane potential (Figure 4f; ●) was well fitted by a straight line (between -80 and $+40$ mV; Figure 4g; ●), and the average E_{rev} was -48.9 ± 6.0 mV (range -60.1 to -42.8 mV; $n = 8$ cells). As above, the decay time course of the spIPSCs was voltage dependent, with slower decay at depolarized potentials (Figure 4f). When I-V relationships were constructed by measuring the current ~ 25 ms after the peak
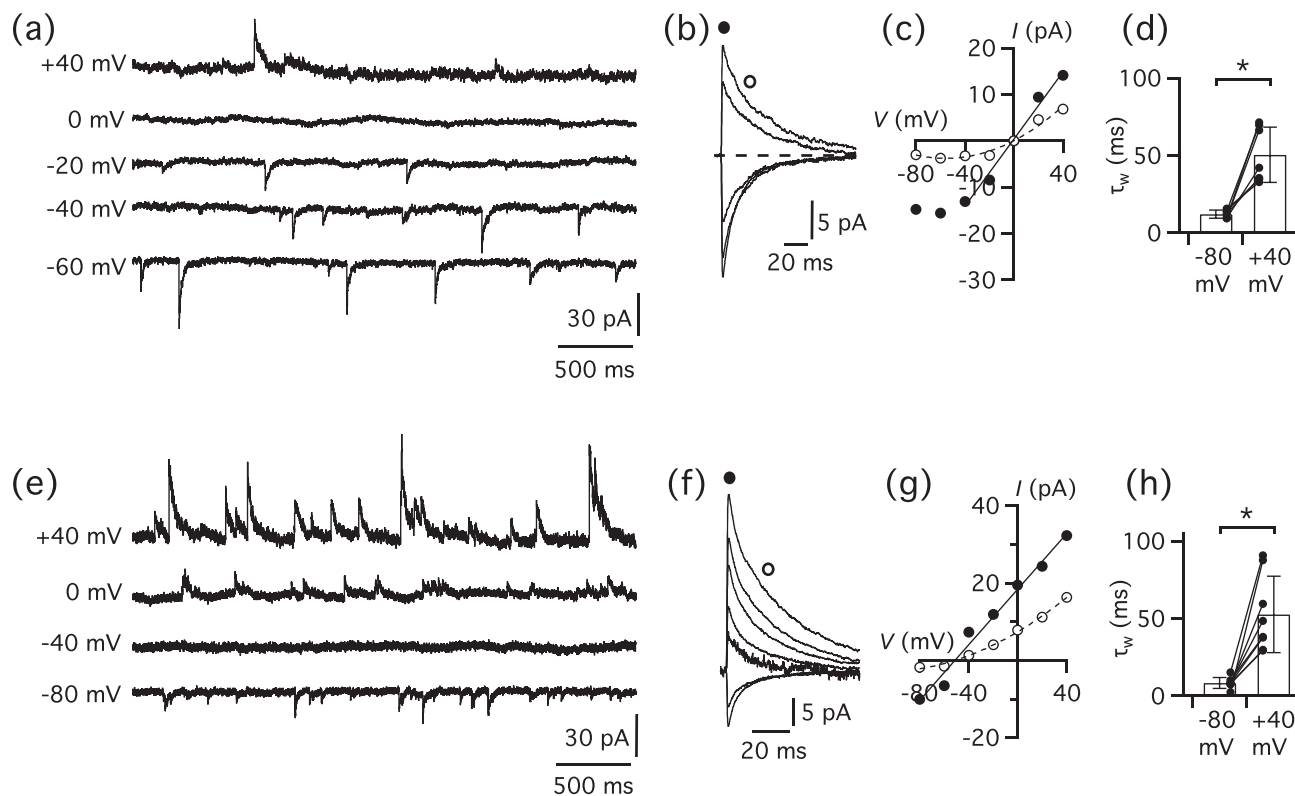
FIGURE 4 Reversal potential and voltage dependence of GABA$_A$ receptor-mediated spIPSCs in A17 amacrine cells. (a) Current traces with spIPSCs in an A17 amacrine cell at five different holding potentials (V_{hold}; $E_{Cl} \sim 3$ mV). Notice outward and inward synaptic currents at positive and negative values of V_{hold}, respectively, and reversal close to zero. Same cell in (a)–(c). (b) Averaged spIPSCs at $V_{hold} = -60, -40, -20, +20$ and $+40$ mV. The individual spIPSCs were aligned at the point of steepest rise before averaging. Notice slower decay at positive than at negative potentials. ● and ○ (peak and decay phase, respectively) indicate time points used for *I-V* relationships in (c). (c) *I-V* relationships of averaged spIPSCs, measured for peak (●) and decay phase (○) of responses in (b), fitted with a straight line (continuous line) and with a third-order polynomial function (broken line), respectively. (d) τ_w for averaged spIPSCs at -80 mV and $+40$ mV. Notice slower decay at $+40$ than at -80 mV ($n = 7$ cells). (e) Current traces with spIPSCs in another A17 amacrine cell at four different values of V_{hold} ($E_{Cl} \sim 43$ mV). Notice outward and inward currents at V_{hold} values more positive and negative than -40 mV, respectively, and no spIPSCs at -40 mV. Same cell in (e)–(g). (f) Averaged spIPSCs at $V_{hold} = -80, -60, -40, -20, 0, +20$ and $+40$ mV. The individual spIPSCs were aligned at the point of steepest rise before averaging. Notice slower decay at depolarized potentials. ● and ○ (peak and decay phase, respectively) indicate time points used for *I-V* relationships in (g). (g) *I-V* relationships of averaged IPSCs, measured for peak (●) and decay phase (○) of responses in (f), fitted with a straight line (continuous line) and with a third-order polynomial function (broken line), respectively. (h) τ_w for averaged IPSCs at -80 mV and $+40$ mV. Notice slower decay at $+40$ than at -80 mV ($n = 8$ cells)

amplitude, the *I-V* relationship again displayed clear outward rectification (data points were fitted with a third-order polynomial function for illustration purposes; Figure 4g; ○). To further analyze the voltage-dependent decay time course, we fitted the decay with a double-exponential function. At $+40$ mV, the average τ_w was 52.7 ± 24.6 ms (range 29.4–90.8 ms), significantly slower than τ_w at -80 mV (8.5 ± 3.5 ms, range 2.5–15.2 ms; $p = 0.0014$, paired *t*-test; $n = 8$ cells; Figure 4h).

Taken together, the above results suggested that E_{rev} for the GABAergic spIPSCs closely follows E_{Cl} and that the corresponding channels display a high selectivity for chloride. A similar voltage-dependent decay time course has been observed for several other types of receptor channels involved in synaptic transmission (e.g. glycine receptors: Gill et al., 2006; Legendre, 1999; AMPA receptors: Glowatzki & Fuchs, 2002; Otis et al., 1996; Veruki et al., 2003; Zhang & Trussell, 1994), but it is unclear whether this is of functional importance in any physiologically relevant condition.
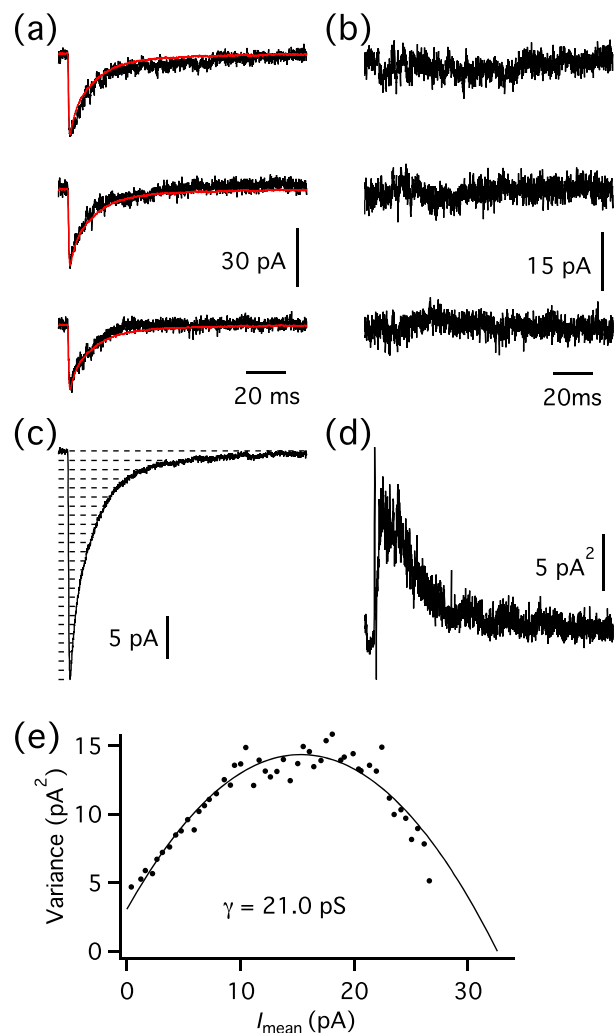
4.6 | Non-stationary noise analysis of GABAergic spontaneous IPSCs in A17 amacrine cells

We used non-stationary noise analysis of GABAergic spIPSCs to estimate the unitary conductance of the synaptic receptor channels (for review, see Hartveit & Veruki, 2007). To reduce the overall influence of

electrotonic filtering, as well as differential electrotonic filtering of spIPSCs generated at different distances from the cell body, we restricted the analysis to cells that met the criteria for kinetic analysis (see above). In addition, to reduce the influence of variations in R_S, we limited the period during which a population of spIPSCs was acquired to 180 s (three consecutive periods of 60 s each). Each of the cells included in the analysis had at least 35 spIPSCs. Due to quantal variability, with the number of receptors available for binding of neurotransmitter varying between individual spIPSCs, as well as variation in the identity of the release sites, we used peak-scaled non-stationary noise analysis. Here, the peak of the ensemble mean waveform is scaled to the peak of each individual spIPSC before the waveforms are subtracted to calculate the ensemble variance (Figure 5). Figure 5a shows three individual spIPSCs, with the peak-scaled mean waveform (generated from the complete ensemble of spIPSCs; $n = 98$ events) overlaid (in red) for each case. The corresponding difference traces are shown in Figure 5b, the ensemble mean in Figure 5c and the ensemble variance in Figure 5d. After binning, the ensemble variance was plotted versus the ensemble mean for corresponding points in time during the decay phase to generate a parabolic curve that was fitted with Equation 3 (Figure 5e). This provided an estimate of the unitary current (i) of 1.47 pA, corresponding to a unitary chord conductance (γ) of 21.0 pS. For nine cells (with 35–141 events), we used peak-scaled non-stationary noise analysis and obtained an average unitary chord conductance of 21.4 ± 4.0 pS (range 16.5–27.9 pS). This corresponded to an average number of channels open at the peak (peak of average current/unitary current) of 17 ± 4 (range 10–26 channels). Based on the estimated value for single-channel conductance, these results are consistent with either an αβδ or αβγ subunit composition (see Section 5).

4.7 | Evidence for the γ subunit in synaptic GABA_A receptors of A17 amacrine cells

The specific subunits that form a GABA_A receptor confer distinct physiological and pharmacological properties (reviewed by Möhler, 2006). There is morphological evidence for the expression of several different types of GABA_A receptor subunits in the inner plexiform layer of rodent retina, including α1–4, α6, β1–3, γ1–2 and δ (Greferath et al., 1995; Gustincich et al., 1999; Gutiérrez et al., 1996; Khan et al., 1996; Wässle et al., 1998). However, except for very few cell types, for example, dopaminergic amacrine cells (Feigenspan et al., 2000),

FIGURE 5 Non-stationary noise analysis of GABA_A receptor-mediated spIPSCs in an A17 amacrine cell. (a) Three individual spIPSCs, in each case with superimposed mean spIPSC (smooth red curves) after peak-scaling mean waveform to each individual spIPSC. (b) Three difference currents calculated from corresponding individual spIPSCs and peak-scaled mean IPSC (in (a)). (c) Ensemble mean IPSC; broken horizontal lines indicate amplitude intervals used for binning mean current and variance (for improved visualization, only every other line has been displayed). (d) Ensemble current variance (without binning) for the spIPSCs; calculated from the difference traces between individual spIPSCs and peak-scaled mean IPSC (as in (b)). (e) Plot of ensemble current variance calculated with peak scaling (d) versus mean current (c) after binning. The time range used for the variance versus mean plot corresponds to data points from the peak of the mean waveform to the end of the decay phase. Data points fitted with Equation 3

there is little evidence to attribute expression of specific GABA_A receptor subunit combinations to specific neurons. For A17 amacrine cells, there is evidence (from cat retina) for GABA_A receptors with β2 and/or β3 subunits (Grünert & Hughes, 1993), but there is no information on

the other subunits that might be present. To functionally investigate the subunit composition of the synaptic $GABA_A$ receptors in A17 amacrines, we performed experiments using pharmacological agents known to have well-defined actions on specific receptor subunits and subunit combinations of $GABA_A$ receptors.

The first agent we used was Zn^{2+}, which differentially blocks $GABA_A$ receptors in a concentration-dependent manner depending on the subunits present. When a γ subunit is present, the resulting receptors are relatively insensitive to low concentrations of Zn^{2+} (Draguhn et al., 1990). From studies with heterologously expressed $GABA_A$ receptors, the IC_{50} for Zn^{2+} has been reported as 88 nM for αβ-containing receptors, 6–16 μM for αβδ-containing receptors and 50–100 μM for αβγ-containing receptors. The specific subunit combination α1βγ is even less sensitive to Zn^{2+}, with an IC_{50} of 300 μM (Draguhn et al., 1990; Smart et al., 1991). Here, we used four concentrations of Zn^{2+} (10 μM, 100 μM, 500 μM and 1 mM) to examine the effect on spIPSCs (in the presence of CNQX, strychnine and TTX). Because of the time required for recording and solution changes, an individual A17 amacrine was typically examined with only two different concentrations of Zn^{2+}, in addition to the control. The cell illustrated in Figure 6a was exposed to 10 and 100 μM Zn^{2+}. There was no obvious effect of 10 μM Zn^{2+} on the frequency or amplitude of spIPSCs (Figure 6a, middle trace). When the cell was exposed to 100 μM Zn^{2+}, however, a reduction of both frequency and amplitude of the spIPSCs could be observed (Figure 6a, bottom trace). For all conditions, we applied the technique of largest amplitude count matching (Stell & Mody, 2002) to compare the average peak spIPSC amplitude recorded during 3-min periods in control and during exposure to Zn^{2+}. For cells exposed to 10 μM Zn^{2+}, there was a small but not statistically significant reduction of the average count-matched amplitude from 25.6 ± 13.8 pA in control to 19.4 ± 6.6 pA in Zn^{2+} (19% decrease; $p = 0.1490$, paired t-test; $n = 5$ cells; Figure 6b). In contrast, in the presence of 100 μM Zn^{2+}, there was a significant reduction of the average count-matched amplitude from 23.8 ± 6.2 pA in control to 13.5 ± 3.5 pA in Zn^{2+} (41% decrease; $p = 0.0174$, paired t-test; $n = 5$ cells; Figure 6b). A significant reduction of the average count-matched amplitude was also seen when Zn^{2+} was applied at the two higher concentrations of 500 μM and 1 mM (Figure 6b). For 500 μM Zn^{2+}, the reduction was from 35.9 ± 4.6 pA (in control) to 11.3 ± 1.1 pA (in Zn^{2+}; 68% decrease; $p = 0.0142$, paired t-test; $n = 3$ cells; Figure 6b), and for 1 mM Zn^{2+}, the reduction was from 50.4 ± 11.9 pA (in control) to 10.6 ± 1.8 pA (in Zn^{2+}; 79% decrease; $p = 0.0234$, paired t-test; $n = 3$ cells; Figure 6b). It should be emphasized, however, that as a

larger number of spIPSCs (recorded in the presence of Zn^{2+}) fall below the level of detection, the average count-matched amplitude in the control condition increases (cf. Figure 6b). The relatively weak amplitude suppression evoked by 10 μM Zn^{2+} (~19%) suggested that these receptors are unlikely to be composed of αβ- or αβδ-containing receptors, for which a much larger reduction would be expected. Instead, our data suggest that a substantial fraction of these synaptic receptors are likely to be composed of αβγ subunits.

4.8 | Evidence for α1 and γ2 subunits in synaptic $GABA_A$ receptors of A17 amacrine cells

We next examined the effect of zolpidem, an agonist at the $GABA_A$ receptor benzodiazepine binding site, with very high affinity for receptors that contain both α1 and γ2 subunits (Pritchett et al., 1989; Pritchett & Seeburg, 1990; Wafford et al., 1993). $GABA_A$ receptors with α2 and α3 subunits have a lower sensitivity to zolpidem, whereas receptors with α4, α5 and α6 subunits are essentially insensitive to zolpidem (reviewed by Möhler, 2006). In addition, $GABA_A$ receptors with either γ1 or γ3 subunits are also essentially insensitive to zolpidem (Dämgen & Lüddens, 1999; Puia et al., 1991). From single-channel recording experiments, we know that benzodiazepines increase the channel open and burst frequency, without a change in the average open and burst duration and with no change in the single-channel conductance (Rogers et al., 1994). Whereas the predominant effect of zolpidem on spIPSCs is to prolong their decay time, zolpidem can also result in increased amplitudes of spIPSCs (Gao & Smith, 2010). To examine the effect of zolpidem, we first recorded spIPSCs in a control condition (in the presence of CNQX, strychnine, TTX and CPP). We then added zolpidem to the bath at a low concentration of 100 nM. At this concentration, zolpidem is expected to influence only receptor channels that contain both the α1 and γ2 subunits (Criswell et al., 1997; Pritchett et al., 1989; Pritchett & Seeburg, 1990).

For the cell illustrated in Figure 6c–e, application of zolpidem at 100 nM resulted in a slight decrease in the frequency of the spIPSCs, from 4.1 Hz in control to 2.8 Hz in zolpidem. However, for a total of five cells tested, zolpidem had no consistent effect on frequency, with a control value of 2.8 ± 1.0 Hz (range 1.7–4.1 Hz) compared with 2.4 ± 0.9 Hz (range 1.4–3.4 Hz) in zolpidem ($p = 0.5236$, paired t-test; Figure 6f). To examine potential changes in peak amplitude, we plotted the cumulative probability distribution of the amplitudes for all events during a 3-min period. For the cell illustrated
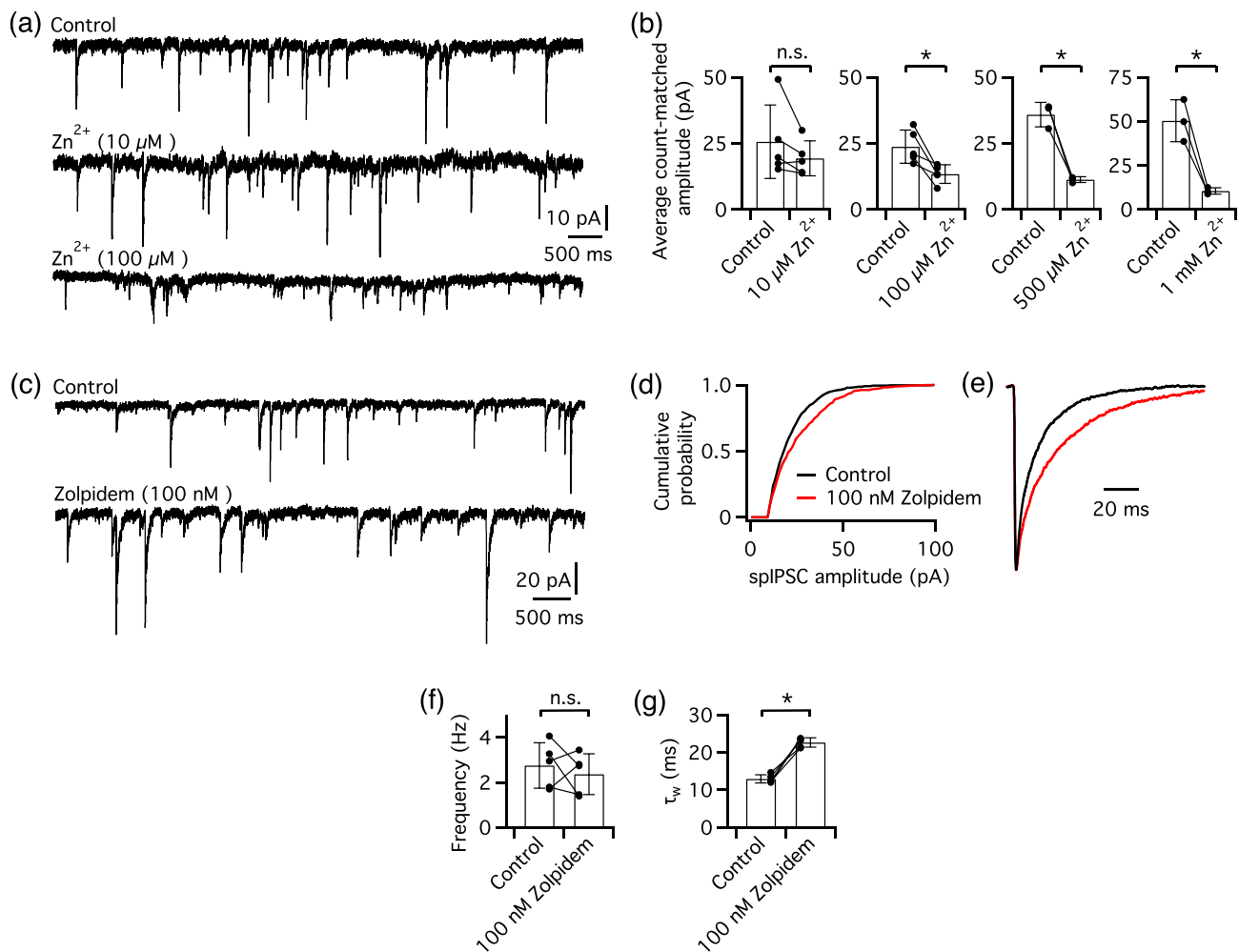
FIGURE 6 Pharmacological properties suggest that GABA$_A$ receptors mediating spIPSCs in A17 amacrine cells contain α1 and γ2 subunits. (a) spIPSCs from an A17 amacrine recorded in the presence of 10 μM CNQX, 300 nM strychnine and 300 nM TTX (upper trace; here and in (b) referred to as 'control') and after adding 10 μM Zn^{2+} (middle trace) or 100 μM Zn^{2+} (lower trace). (b) Average count-matched peak amplitude of spIPSCs for cells recorded in control and in the presence of 10 μM Zn^{2+} (left; $n = 5$ cells); cells recorded in control and in the presence of 100 μM Zn^{2+} (middle left; $n = 5$ cells); cells recorded in control and in the presence of 500 μM Zn^{2+} (middle right; $n = 3$ cells); cells recorded in control and in the presence of 1 mM Zn^{2+} (right; $n = 3$ cells). Notice increasing block of spIPSCs with increasing concentration of Zn^{2+}. (c) spIPSCs from an A17 amacrine recorded in the presence of 10 μM CNQX, 300 nM strychnine, 20 μM CPP and 300 nM TTX (upper trace; here and in (d)–(g) referred to as 'control') and after adding 100 nM zolpidem (lower trace). Notice increase in amplitude of spIPSCs in the presence of zolpidem. Same cell in (c)–(e). (d) Zolpidem (100 nM) increases the peak amplitude of spIPSCs in the A17 amacrine cell, as illustrated by the cumulative probability density (relative frequency) distributions for the population of events recorded in the control condition (black line; $n = 319$ events) and after adding zolpidem (red line; $n = 262$ events). (e) Normalized average waveforms of spIPSCs (as in (d)) in control (black) and in zolpidem (red). Notice slower decay time course in the presence of zolpidem. (f) Frequency of spIPSCs in control and in the presence of 100 nM zolpidem ($n = 5$ cells). (g) τ_w for averaged spIPSCs (decay phase fitted with double-exponential function) in control and in the presence of 100 nM zolpidem (same cells as in (f))

in Figure 6c–e, there was a significant increase in amplitude following addition of zolpidem at 100 nM ($p < 0.0001$, Kolmogorov–Smirnov test; Figure 6d). A statistically significant increase in amplitude was observed for four of the five cells ($p < 0.0001$, Kolmogorov–Smirnov test). For the fifth cell, the difference in

amplitude between control and zolpidem was not statistically significant ($p = 0.0583$, Kolmogorov–Smirnov test). To investigate the effect of zolpidem on the decay time course, we averaged the waveforms from well-separated events and calculated τ_w after fitting the decay phase with a double-exponential function. For the cell

illustrated in Figure 6c–e, zolpidem slowed the decay kinetics, with a change of τ_w from 12 ms in the control condition to 24 ms in zolpidem (Figure 6e). For the five cells, 100 nM zolpidem evoked a significant increase in the decay time course, from an average $\tau_w = 13.0 \pm 1.1$ ms (range 12.0–14.7 ms) in control to an average $\tau_w = 22.7 \pm 1.2$ ms (range 21.3–23.8 ms) in zolpidem ($p = 0.0004$, paired t-test; Figure 6g).

Our pharmacological experiments suggested that a relatively high concentration of Zn^{2+} was required for suppression of the A17 spIPSCs, and our noise analysis experiments suggested a single-channel conductance of ~21 pS. Taken together, these results predict an αβγ composition, as opposed to an αβ or an αβδ composition (see Section 5). In addition, the pronounced slowing of decay kinetics evoked by zolpidem (in the low nM range) strongly suggested that the subunit composition can be narrowed down to an α1βγ2 composition (Pritchett & Seeburg, 1990; Wafford et al., 1993; for review, see Möhler, 2006). With regard to the identity of the β subunit, discrimination of the molecular composition of the synaptic GABA$_A$ receptors in A17 amacrines based solely on pharmacological experiments is challenging and prone to misinterpretation, unless combined with in situ hybridization or immunohistochemical studies (e.g. Feigenspan et al., 2000). Earlier immunolabelling studies suggested that the β2 and/or β3 subunit is present in A17s (Grünert & Hughes, 1993), but from our results in the current study, it is not possible to exclude the presence of the β1 subunit. In conclusion, our results suggest that the majority of synaptic GABA$_A$ receptors of A17 amacrine cells are composed of α1βγ2 subunits, potentially with either β2 or β3.

4.9 | Kinetic properties of GABA$_A$ receptors in patches from A17 amacrine cells

To investigate the deactivation and desensitization kinetics of the GABA$_A$ receptor channels under controlled conditions, we isolated outside-out patches from the cell bodies of A17 amacrines and evoked responses by application of GABA via ultra-fast perfusion. In such experiments, the concentration of agonist can be changed with a rise time of a few hundred microseconds, effectively mimicking the concentration profile of neurotransmitter thought to be generated in the synaptic cleft following presynaptic exocytosis (Clements, 1996; Scimemi & Beato, 2009). For the A17 amacrine cell, there are to our knowledge no reports of synapses made onto the cell body, but from previous work in our laboratory, there is evidence for ionotropic GABA receptors (presumably

GABA$_A$) in nucleated patches isolated from these cells (Zhou et al., 2016). The extent to which the functional properties of these somatic extrasynaptic GABA$_A$ receptors resemble those of synaptic receptors is not known.

We first tested whether GABA-evoked responses in patches are mediated by GABA$_A$ receptors. Nucleated ($n = 3$) and outside-out ($n = 1$) patches were pulled from the soma of A17 amacrines, and brief (5 ms) pulses of GABA (3 mM) were applied from one barrel of a theta-tube pipette. After establishing baseline responses to GABA, the solution in the second barrel of the theta-tube pipette was switched from control to a solution containing SR95531 (3 μM). As illustrated for the nucleated patch in Figure 7a, SR95531 almost completely blocked the GABA-evoked current. Without SR95531, the peak amplitude was 1.5 nA, and with SR95531, it was 39 pA (a reduction of 97%). After switching back to control solution and washing out SR95531, the response to GABA fully recovered (Figure 7a). For all patches tested, SR95531 reduced the GABA-evoked current by $97 \pm 2\%$ ($n = 4$ patches), suggesting that it was mediated by GABA$_A$ receptors. Because SR95531 is a competitive antagonist, the combination of a high concentration of GABA and relatively long pulse duration (compared with the typical duration of transmitter in the synaptic cleft after presynaptic exocytosis) probably explains why the response to GABA was not completely eliminated.

We next investigated the deactivation kinetics of the GABA$_A$ receptor-mediated responses by applying brief (3 ms) pulses of GABA (3 mM). Figure 7b illustrates the average response of an outside-out patch from an A17 amacrine cell ($n = 9$ repetitions). The response rose rapidly to a peak of ~250 pA with a 10%–90% rise time of 444 μs (20%–80% rise time of 376 μs). After reaching the peak, the response decayed back to baseline, initially with a fast time course and then more slowly. This decay corresponds to receptor deactivation, that is, closure of channels after removal of GABA. The decay time course was well fitted by a triple-exponential function with $\tau_1 = 7.8$ ms, $\tau_2 = 51$ ms and $\tau_3 = 160$ ms, with amplitude contributions of ~59%, ~29% and ~11%, respectively. The weighted time constant of decay (τ_w) was 38 ms.

For nine outside-out patches examined with brief (2–3 ms) pulses of GABA (3 mM; $n = 3$–35 repetitions for each patch), the average peak amplitude was 154 ± 119 pA (range 24–344 pA). The average 10%–90% rise time was 448 ± 84 μs (range 353–603 μs), and the 20%–80% rise time was 299 ± 58 μs (range 235–384 μs). For 7/9 outside-out patches tested with brief pulses of GABA, it was necessary to fit the deactivation time course with a triple-exponential function (as opposed to either single- or double-exponential functions) to obtain a good fit, and we therefore report the results for triple-
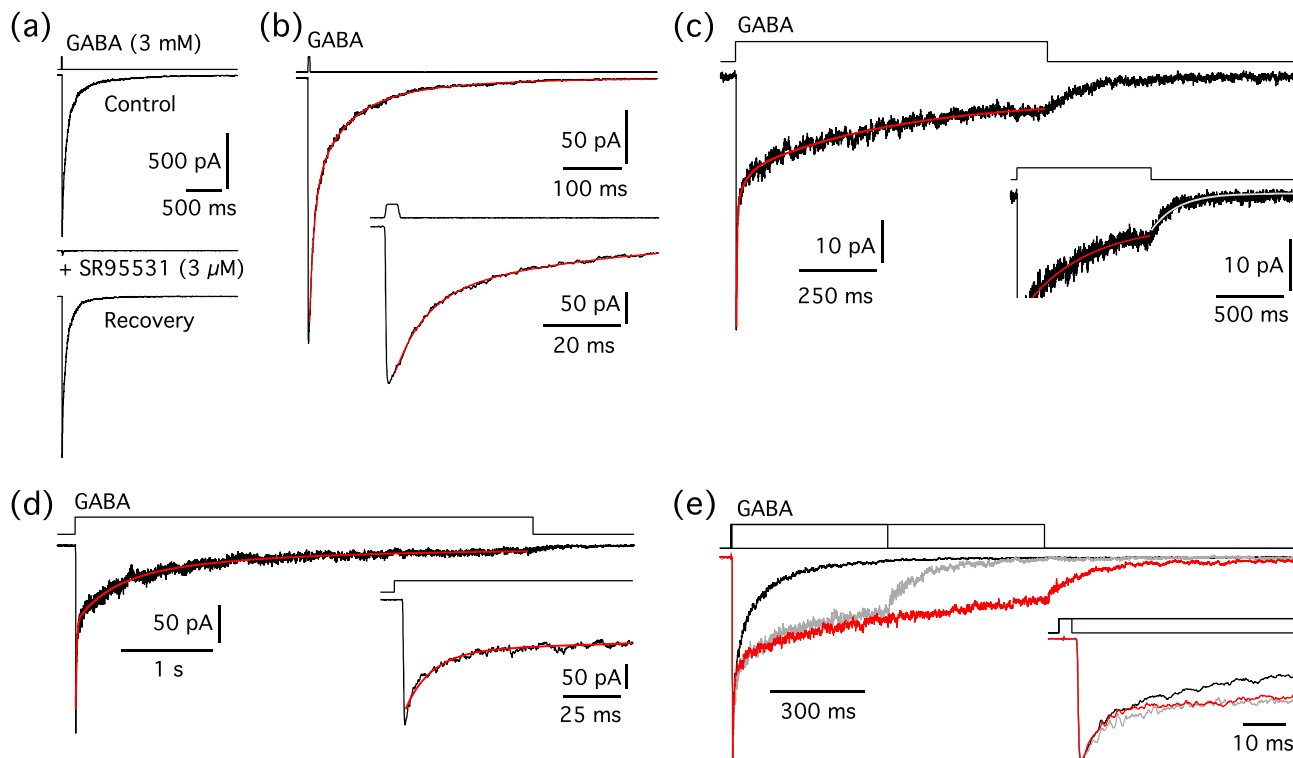
FIGURE 7 Deactivation and desensitization kinetics of $GABA_A$ receptors in A17 amacrine cell patches. (a) Three individual responses (single trials) of a nucleated patch to 5-ms application of GABA (3 mM) in control (upper trace), after exposure to 3 µM SR95531 (middle trace) and after washout (bottom trace). Notice almost complete block of GABA-evoked response by SR95531, followed by full recovery after washout. Here and later, the black line above the current responses illustrates either the exchange time course (measured as a change in liquid junction current with an open-tip pipette after breaking the patch) or, alternatively, the square wave voltage pulse from the digital-to-analog output of the ITC-16 interface (of the patch-clamp amplifier) when measurement of the exchange time was not successful. Notice that this latter waveform precedes the patch response by a few milliseconds. For nucleated patches, the true exchange time will be slower than the measured exchange time. (b) Response of outside-out patch (average of nine repetitions) to brief (3 ms), ultra-fast application of GABA (3 mM), overlaid with triple-exponential fit (red line) to the deactivation decay phase. Inset illustrates expanded view of response around peak and initial decay phase. (c) Response of outside-out patch (average of 17 repetitions) to long (1 s), ultra-fast application of GABA (3 mM), overlaid with triple-exponential fit (red line) to the desensitization decay phase. Inset illustrates same response, overlaid with single-exponential fit (white line) to deactivation decay phase following removal of GABA. (d) Response of outside-out patch (average of two repetitions) to long (5 s), ultra-fast application of GABA (3 mM), overlaid with triple-exponential fit (red line) to the desensitization decay phase. Inset illustrates expanded view of response around peak and initial decay phase. (e) Normalized responses of outside-out patch to a series of applications of GABA (3 mM) of variable duration (3 ms, black trace; 500 ms, gray trace; 1 s, red trace). Each trace is the average of five repetitions. Notice how the overlaid responses illustrate the difference between the faster deactivation and the slower desensitization kinetics, including the transition from desensitization to deactivation for the two longer pulse durations. Inset illustrates the similar kinetics for the initial decay phase, irrespective of the duration of GABA application

exponential fits for all nine patches. The average τ_1 was 5.3 ± 2.0 ms (range 2.9–7.8 ms; $55 \pm 7\%$ amplitude contribution), the average τ_2 was 48.2 ± 9.6 ms (range 30–59 ms; $32 \pm 6\%$ amplitude contribution), and the average τ_3 was 187 ± 43 ms (127–250 ms; $13 \pm 5\%$ amplitude contribution). The average τ_w was 42.1 ± 7.5 ms (range 32–52 ms). When compared with the decay time course of the A17 spIPSCs, the deactivation kinetics of the $GABA_A$ receptor-mediated responses of outside-out patches to brief pulses of GABA are relatively similar, except for the final decay

that is slower for the patch responses. Interestingly, τ_{fast} for the spIPSC decay and τ_1 for the patch decay are very similar. It is possible that the slower decay of the patch responses could be related to the duration of exposure to GABA. Even the briefest pulses we were able to obtain (2–3 ms) are most likely longer than the effective duration of the synaptic transient of GABA. As demonstrated by Jones and Westbrook (1995) (for review, see Jones & Westbrook, 1996), even brief exposure to GABA can drive receptor channels into desensitized states and when they

return from these states there is a possibility that the channels will (re)open before GABA finally unbinds and the channels close. The decay time course of spPSCs is generally thought to be determined by the deactivation, as opposed to the desensitization, kinetics of the receptor channels (reviewed by Hartveit & Veruki, 2007). Taken together, our results suggest that with respect to decay kinetics, there may be some degree of overlap between the somatic extrasynaptic receptors and the synaptic receptors.

We next investigated the receptor desensitization kinetics that reflect the closure of channels in the maintained presence of agonist. To study the time course and extent of desensitization of GABA_A receptors in A17 somatic patches, we applied longer pulses (1 s) of GABA (3 mM). For the patch illustrated in Figure 7c, application of GABA ($n = 17$ repetitions) evoked a rapidly increasing response, followed by a decay that could be well fitted with a triple-exponential function with $\tau_1 = 2.4$ ms, $\tau_2 = 27$ ms and $\tau_3 = 480$ ms, with amplitude contributions of ~62%, ~12% and ~26%, respectively. At the end of the 1-s pulse, the extent of desensitization was pronounced, with a response amplitude that was ~14% of the initial peak amplitude. For eight patches tested with 1-s pulses, the average τ_1 was 3.7 ± 2.4 ms (range 1.5–8.5 ms; $57 \pm 16\%$ amplitude contribution), the average τ_2 was 59 ± 41 ms (range 13–140 ms; $15 \pm 9\%$ amplitude contribution), and the average τ_3 was 673 ± 315 ms (range 302–1153 ms; $27 \pm 11\%$ amplitude contribution). The average τ_w was 215 ± 154 ms (range 42–437 ms). At the end of the 1-s pulse of GABA, the average response amplitude was $12.5 \pm 6.4\%$ of the initial peak amplitude (range 2.5–21%). Following the pulse, when GABA was rapidly removed from the patch, the decay time course changed from desensitization to deactivation (Figure 7c), with a time course that was well fitted by a single-exponential function with $\tau_{decay} = 191$ ms. For eight patches analysed in this way, the average τ_{decay} for deactivation following a 1-s pulse was 301 ± 178 ms (range 134–636 ms).

To investigate whether the response at the end of a 1-s GABA pulse represented a true equilibrium response, or if the desensitization would increase with continued exposure to GABA, we also examined the response to a 5-s long pulse ($n = 4$ patches). For the patch illustrated in Figure 7d, the desensitization continued slowly in the period from 1 to 5 s. At the end of the 5-s pulse, the response (~7 pA) was ~3% of the initial peak amplitude. For the four patches tested in this way, the average steady-state response was $2.86 \pm 0.70\%$ (range 1.9–3.5%) of the peak. Although the concentration of GABA used here is several-fold larger than the presumed ambient concentration of GABA in the extrasynaptic environment (~1 μM; Juhász et al., 1997), this suggested that extrasynaptic GABA_A receptors on the soma could mediate a small,

tonically active current. The time course of desensitization evoked by 5-s GABA pulses required a triple-exponential function to be well fitted, with $\tau_1 = 11.6 \pm 3.3$ ms (range 7.0–14.1 ms; $47 \pm 8\%$ amplitude contribution), $\tau_2 = 444 \pm 303$ ms (range 105–840 ms; $25 \pm 7\%$ amplitude contribution) and $\tau_3 = 1.8 \pm 0.6$ s (range 1.1–2.5 s; $27 \pm 13\%$ amplitude contribution). The average τ_w was 587 ± 181 ms (range 395–789 ms).

For individual outside-out patches tested with both brief and long pulses of GABA (durations ~3 ms, 500 ms and 1 s), we could directly observe that the time course of desensitization was similar for different pulse durations (Figure 7e; 0.5 and 1 s). When GABA was removed from the patch, the decay changed immediately from the slow desensitization to the faster deactivation (Figure 7e). For the example illustrated in Figure 7e, the response waveforms were normalized by the peak amplitudes for adequate visualization and comparison of the decay time courses.

4.10 | Non-stationary noise analysis for estimating the single-channel conductance of GABA_A receptor channels in outside-out patches

To extend the comparison of functional properties between these receptors, we used non-stationary noise analysis to estimate the single-channel current and maximum P_{open} of the somatic GABA_A receptor channels (Figure 8). Responses were evoked by ultra-fast application of brief (2–3 ms) pulses of GABA (3 mM) to outside-out patches. Figure 8a shows three consecutive individual responses evoked by GABA in the same patch. Because moderate response rundown was observed for ~50% of the patches, we estimated the ensemble variance (Figure 8d) by calculating the differences between consecutive responses (Figure 8b; Heinemann & Conti, 1992). After binning, the ensemble mean waveform (Figure 8c) was used to generate a variance versus mean plot, corresponding to the decay phase of the response ($n = 35$ repetitions; Figure 8e). When the data points were fitted with the parabolic function of Equation 3 (Figure 8e), we obtained an apparent single-channel current of 1.38 pA, corresponding to an apparent single-channel chord conductance of 23.0 pS. The number of available channels in the patch was estimated as 72, corresponding to a maximum P_{open} at the peak response of 0.57 (Figure 8e). For nine patches tested with GABA in this way, the mean single-channel chord conductance was 24.7 ± 1.3 pS (range 20.2–31.3 pS), and the mean number of available channels was 134 ± 30 (range 24–291). The average maximum P_{open} was 0.65 ± 0.05 (range 0.46–0.91). The estimated value for
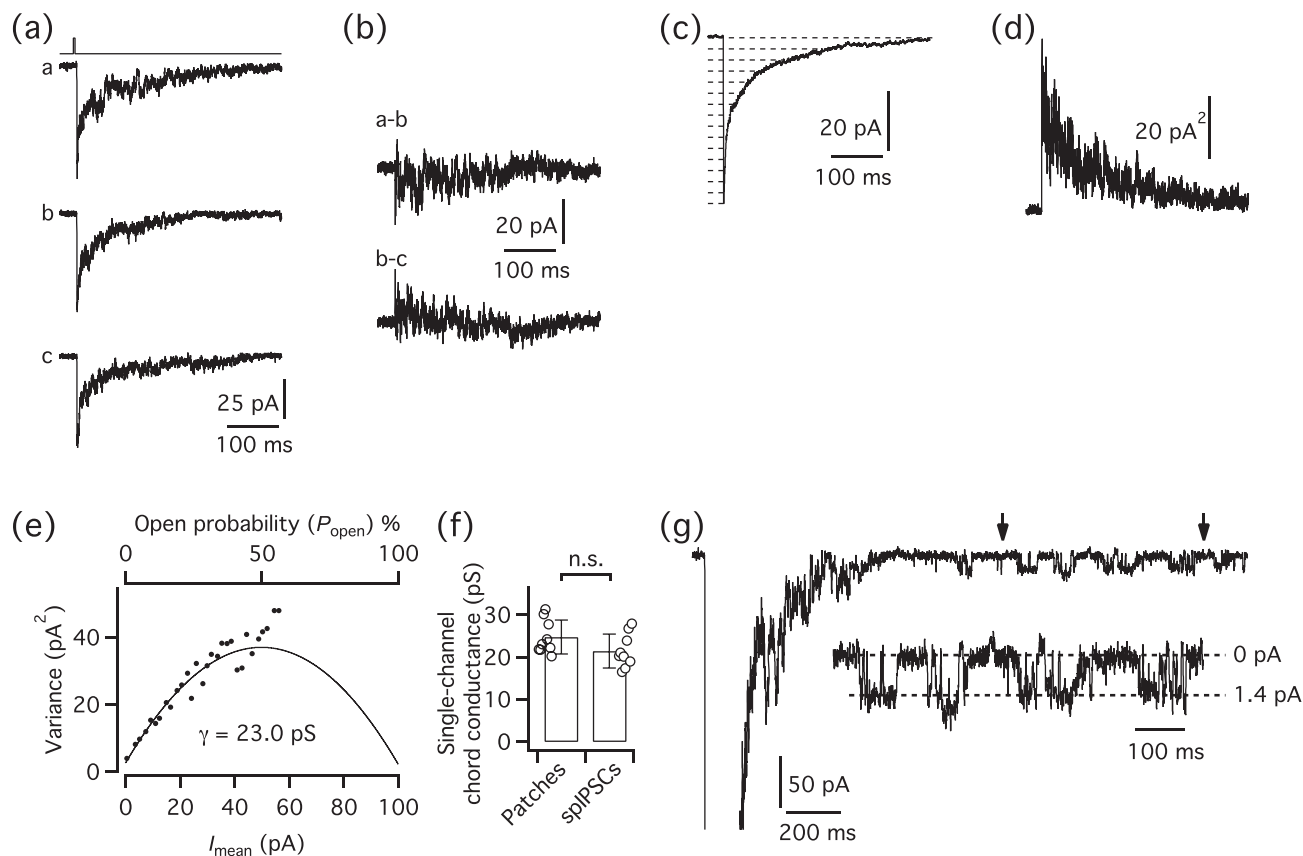
FIGURE 8 Non-stationary noise analysis of GABA-evoked responses in an outside-out patch from an A17 amacrine cell. (a) Three successive records obtained by application of brief (3 ms) pulses of GABA (3 mM) to an outside-out patch. (b) Pairwise difference currents calculated from pairs of successive responses in (a) (as indicated). (c) Mean current of all GABA-evoked responses ($n = 35$ repetitions). Broken horizontal lines indicate amplitude intervals used for binning mean current and variance (for improved visualization, only every other line has been displayed). (d) Ensemble current variance (no binning) for the GABA-evoked responses, calculated from the pairwise difference currents between successive responses (as in (b)). (e) Plot of ensemble current variance (d) versus mean current (I_{mean}; (c)). Data points correspond to time period from peak of the mean response waveform to the end of the decay phase. The data points were fitted with a parabolic function (Equation 3). (f) Single-channel chord conductances obtained by non-stationary noise analysis of outside-out patches ($n = 9$ patches) and spIPSCs ($n = 9$ cells). (g) Current response (single trial) evoked by brief (3 ms) pulse of GABA (3 mM) to an outside-out patch. The peak of the response has been truncated for better visualization of the single-channel gating evoked by application of GABA. Inset displays the latter part of the response (between vertical arrows) at an expanded time scale; broken lines indicate baseline current (0 pA; leak current has been subtracted) and inward current amplitude during channel openings

the single-channel chord conductance of the extrasynaptic GABA$_A$ receptor channels in somatic patches was not significantly different from that estimated (from spIPSCs) for synaptic GABA$_A$ receptors (21.4 pS; $p = 0.1014$, unpaired t-test; Figure 8f).

4.11 | Direct observations of single-channel gating in patch responses

The estimates from non-stationary noise analysis are likely to represent weighted averages of different conductance levels of different channels or different sub-conductance states of the same types of channel. For several outside-out patches with low noise levels, discrete transitions

between open and closed states could be observed during the late decay phase of individual responses when P_{open} was low (Figure 8g). Channel openings, ranging between 1.2 and 2.5 pA (corresponding to chord conductance values of 20.1–42.3 pS), were observed in eight different patches ($n = 72$ measurements).

4.12 | Evidence for α2/α3 and γ2 subunits in the somatic GABA$_A$ receptors of A17 amacrine cells

Although the single-channel conductances are very similar for GABA$_A$ receptors mediating spIPSCs and somatic patch responses, the deactivation time course of patch

responses evoked by a brief GABA pulse (τ_w ~40 ms) is slower than the decay time course of spIPSCs (τ_w ~15 ms), suggesting that the subunit composition of the synaptic and extrasynaptic (somatic) receptors differ from each other. Alternatively, the kinetic differences could depend on differences in the phosphorylation state, the extent of palmitoylation or other modulatory mechanisms (Jones & Westbrook, 1997; Keller et al., 2004). The results from noise analysis and direct observations of single-channel openings in patch responses make it very unlikely that the somatic extrasynaptic GABA$_A$ receptors contain only α and β subunits, as such receptors have a single-channel conductance of ~11–15 pS (Angelotti & Macdonald, 1993; Brickley et al., 1999; Fisher & Macdonald, 1997; Mortensen & Smart, 2006). To further explore the subunit composition of the somatic extrasynaptic receptors, we performed a series of pharmacological experiments. As in the patch experiments reported above, one barrel of the theta-tube application pipette contained 3 mM GABA. The other barrel contained the standard HEPES-buffered solution (to obtain baseline control responses) and could be changed to the same solution with the pharmacological agent to be tested. The pharmacological experiments used both conventional outside-out patches as well as nucleated patches (to increase the response amplitude and reduce rundown) and GABA (3 mM) was applied with 5-ms-long pulses.

To examine the effect of Zn^{2+}, GABA responses were evoked first in the control condition and then after exposing the patch to different concentrations of Zn^{2+}. As illustrated by the time series of patch responses in Figure 9a, 10 μM Zn^{2+} caused a clear suppression of the GABA-evoked response (measured as the peak amplitude), which was reversed after washout of Zn^{2+}. For each condition (control, 10 μM Zn^{2+}, washout), we averaged three successive responses and overlaid the waveforms to compare the responses (Figure 9b). For this patch, 10 μM Zn^{2+} reduced the peak amplitude of the response from 161 to 109 pA, a decrease of 32% (Figure 9b). For a total of six outside-out patches, 10 μM Zn^{2+} reduced the amplitude of GABA-evoked responses by 54 ± 26% (range 28%–83%) relative to control (Figure 9c). For patches exposed to 100 and 500 μM Zn^{2+}, the response reduction was 89 ± 16% (range 61%–98%; $n = 5$ patches) and 95 ± 9% (range 79%–100%; $n = 5$ patches), respectively (Figure 9c). The responses evoked in the presence of 10 μM Zn^{2+} were sufficiently large that the decay kinetics could be adequately analysed. Compared with control, there was no significant change in the rise time (neither 10%–90% nor 20%–80%) or the decay time course ($p > 0.14$, paired t-tests; $n = 6$ patches). The pronounced suppression by Zn^{2+}, even at 10 μM, suggested that the somatic extrasynaptic GABA$_A$

receptors are unlikely to contain GABA$_A$ receptors that include the α1 subunit (see comments above for the corresponding analysis of spIPSCs).

As described above, 100 nM zolpidem markedly slowed the decay kinetics of spIPSCs in all cells and increased the peak amplitudes of the spIPSCs for most cells. We examined the effect of zolpidem on GABA-evoked responses in patches at concentrations of 100 nM and 1 μM (Figure 9d–k) using the same methodology as for Zn^{2+}. For the time series of patch responses in Figure 9d, 100 nM zolpidem had little or no effect on the peak amplitude or the decay time course, as illustrated by the overlaid responses in Figure 9e. Similar results were observed for a total of four patches, with no difference of the peak amplitude between the control condition (1.11 ± 0.31 nA) and 100 nM zolpidem (1.13 ± 0.31 nA; $p = 0.6270$, paired t-test; Figure 9f). There was also no change of the decay time course, with $\tau_w = 34.9 \pm 8.7$ ms in control and $\tau_w = 30.7 \pm 8.0$ ms in 100 nM zolpidem ($p = 0.1341$, paired t-test; Figure 9g).

When we examined the effect of 1 μM zolpidem, there was little change of the peak amplitude, as illustrated by the time series of patch responses in Figure 9h and the averaged and overlaid response waveforms for the same patch in Figure 9i. In contrast, however, 1 μM zolpidem slowed the decay time course from $\tau_w = 64$ ms in control to $\tau_w = 114$ ms (Figure 9i). Similar results were observed for a total of four patches tested with 1 μM zolpidem, with no difference of the peak amplitude between the control condition (1.81 ± 0.47 nA) and 1 μM zolpidem (1.99 ± 0.57 nA; $p = 0.0833$, paired t-test; Figure 9j). In contrast, the decay time course became significantly slower, with $\tau_w = 57 \pm 13$ ms in control and $\tau_w = 92 \pm 22$ ms in 1 μM zolpidem ($p = 0.0082$, paired t-test; Figure 9k). Whereas the lack of effect of 100 nM zolpidem suggested that the somatic extrasynaptic GABA$_A$ receptors are unlikely to contain the α1 subunit (Criswell et al., 1997; Pritchett et al., 1989), the ability of 1 μM zolpidem to slow the decay kinetics of the patch responses suggested the presence of the γ2 subunit (Pritchett et al., 1989) together with the α2 and/or the α3 subunit, as α4, α5 and α6 are all insensitive to zolpidem (Criswell et al., 1997). In addition, the α5 has not been found in rat retina (Wässle et al., 1998).

Taken together, our results with Zn^{2+} and zolpidem suggested that the synaptic and the somatic GABA$_A$ receptors on A17 amacrines have a different subunit composition. Although both receptor populations seem to contain the γ2 subunit, the synaptic receptors are likely to contain the α1 subunit, whereas the somatic receptors are likely to contain the α2 and/or the α3 subunit.
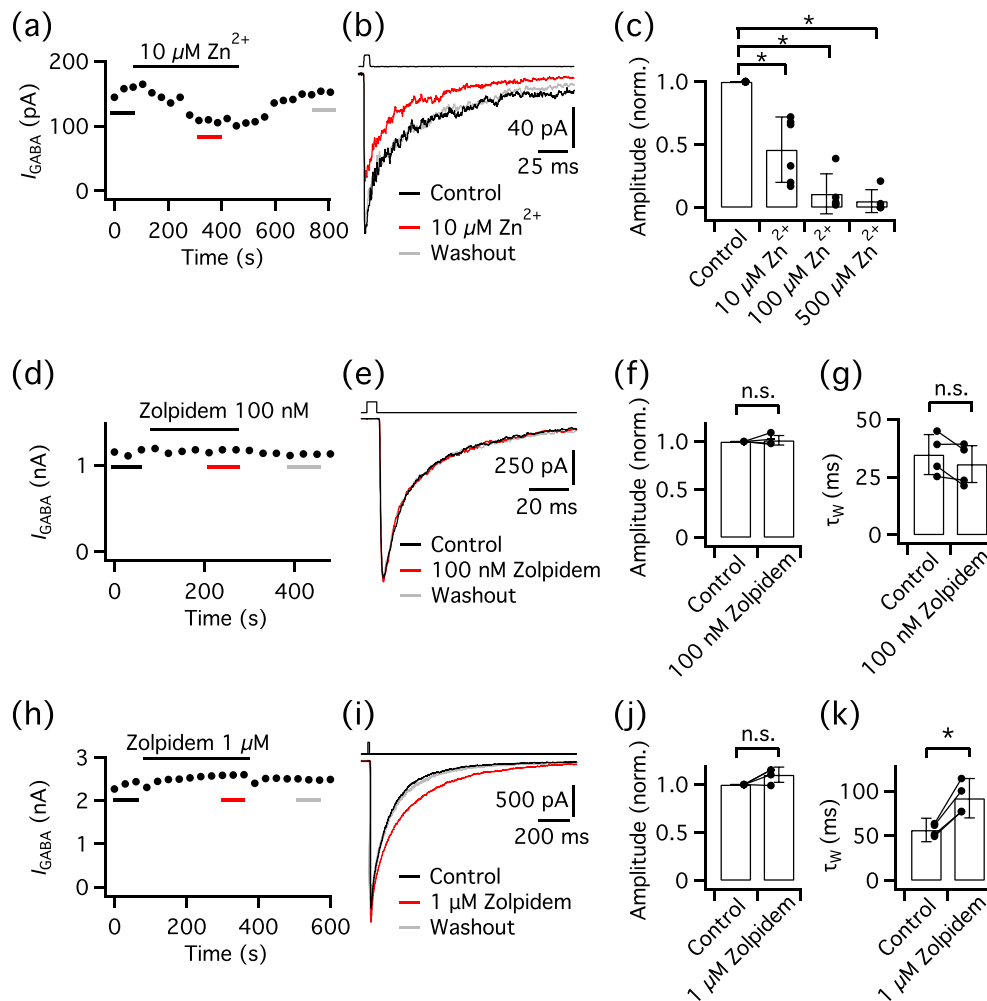
FIGURE 9 Pharmacological properties suggest that somatic extrasynaptic GABA$_A$ receptors of A17 amacrine cells contain α2/α3 and γ2 subunits. (a) Peak amplitude of individual responses evoked in an outside-out patch by application of pulses (5 ms) of GABA (3 mM) at 30-s intervals. Notice the suppression of GABA-evoked responses during addition of 10 μM Zn^{2+}. Here and in (d) and (h), the responses corresponding to data points marked by the short horizontal line for each condition (black, control; red, pharmacological agent; grey, wash) have been averaged and overlaid in a separate panel ((b), (e), (i)). (b) Responses (average of three repetitions) evoked by GABA (same patch as in (a)) in control (black), in 10 μM Zn^{2+} (red) and following washout of Zn^{2+} (grey). (c) Normalized peak amplitudes of GABA-evoked patch responses in control and following application of Zn^{2+} at 10 μM ($n = 6$ patches), 100 μM ($n = 5$ patches) and 500 μM ($n = 5$ patches). Notice increasing block of response with increasing concentration of Zn^{2+}. Some but not all patches were tested with more than a single concentration of Zn^{2+}. (d) Peak amplitude of individual responses evoked in a nucleated patch from the same A17 amacrine cell by application of pulses (5 ms) of GABA (3 mM) at 30-s intervals. Notice that exposure to 100 nM zolpidem does not change the response amplitude. (e) Responses (average of three repetitions) evoked by GABA (same patch as in (d)) in control (black), in 10 nM zolpidem (red) and following washout of zolpidem (grey). Notice that zolpidem does not change the response amplitude or the decay time course. (f) Normalized peak amplitudes of GABA-evoked patch responses in control and following application of 100 nM zolpidem ($n = 4$ patches). Notice that there is no significant change in zolpidem. (g) τ$_w$ for GABA-evoked patch responses (decay phase fitted with triple-exponential function) in control and in the presence of 100 nM zolpidem (same patches as in (f)). Notice that there is no significant change in zolpidem. (h) Peak amplitude of individual responses evoked in a nucleated patch from the same A17 amacrine cell by application of pulses (5 μs) of GABA (3 mM) at 30-s intervals. Notice that exposure to 1 μM zolpidem evokes a small increase of the response amplitude. (i) Responses (average of three repetitions) evoked by GABA (same patch as in (h)) in control (black), in 1 μM zolpidem (red) and following washout of zolpidem (grey). Notice that zolpidem evokes a small increase of the peak amplitude and a marked slowing of the decay time course that reverses after washout of zolpidem. (j) Normalized peak amplitudes of GABA-evoked patch responses in control and following application of 1 μM zolpidem ($n = 4$ patches). Notice that there is no significant change in zolpidem. (k) τ$_w$ for GABA-evoked patch responses (decay phase fitted with triple-exponential function) in control and in the presence of 1 μM zolpidem (same patches as in (j)). Notice significant increase of τ$_w$ in 1 μM zolpidem

4.13 | No evidence for the presence of the δ subunit in somatic GABA$_A$ receptors of A17 amacrine cells

Extrasynaptic GABA$_A$ receptors that mediate tonic currents are typically composed of αβ, αβδ or α5βγ subunit combinations (Farrant & Nusser, 2005; Mortensen & Smart, 2006). However, from our estimates of single-channel conductance values of GABA$_A$ receptors in patches, we can likely rule out an αβ composition and the α5 subunit has not been detected in rat retina (Wässle et al., 1998). To examine whether the somatic receptors contain a δ subunit, we used the GABA$_A$ receptor agonist THIP, which has a high selectivity for receptors containing the δ subunit when used at concentrations ≤1 μM (Jia et al., 2005; Marowsky & Vogt, 2014; Meera et al., 2011; Stórustovu & Ebert, 2003, 2006).

We recorded from nucleated patches and used a theta-tube pipette to apply 1-s pulses of THIP at a concentration of 1, 5 or 10 μM. For the patches illustrated in Figure 10, application of 1 μM THIP did not evoke a measurable response and had no effect on the membrane noise to suggest an increase in channel gating. In contrast, application of THIP at both 5 and 10 μM evoked low-amplitude, sustained inward currents (~6 and ~10 pA, respectively), accompanied by markedly increased membrane noise. Similar results were observed for all patches tested. For 1 μM THIP, there was no evoked current and no increase of membrane noise ($n = 5$ patches). For 5 μM THIP, the average inward current amplitude was 6.5 ± 3.3 pA (range 4.1–8.6 pA; $n = 4$ patches), and for 10 μM, the average inward current amplitude was 10.6 ± 2.4 pA (range 8.4–13; $n = 3$ patches). The lack of response evoked by 1 μM THIP suggested that the δ subunit is not present in the somatic GABA$_A$ receptors expressed by A17 amacrine cells.
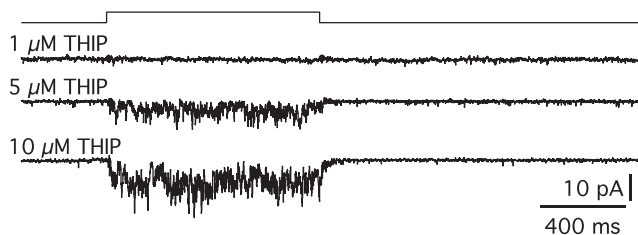
FIGURE 10 No evidence for the δ subunit in somatic GABA$_A$ receptors of A17 amacrine cells. Responses of nucleated patches evoked by 1-s application of THIP at 1, 5 and 10 μM (each trace represents a single trial and a separate patch). Notice that THIP evokes an inward current and increase in membrane current noise at 5 and 10 μM, but not at 1 μM

5 | DISCUSSION

From previous work with puffer application of pharmacological agents to neurons in slices, there is evidence that A17 amacrine cells express both GABA and glycine receptors (Majumdar et al., 2009; Menger & Wässle, 2000; Zhou et al., 2016). Such experiments, however, do not reveal if the receptors are synaptic or extrasynaptic, and almost nothing is known about the molecular specificity (e.g. subunit composition) of the receptors. The demonstration of a synaptic localization of GABA$_A$ receptors on A17 amacrines, as well as information about the functional properties and molecular composition of the receptor subunits, is important for understanding the functional role of inhibitory input for signal integration in these cells. In the case of GABA$_A$ receptors, there are 19 different subunits (α1–6, β1–3, γ1–3, δ, ε, θ, π and ρ1–3) that can be combined to form different variants of the heteropentameric receptors found in different cells and regions of the CNS. Synaptic GABA$_A$ receptors in the CNS are usually constructed from two α subunits, two β subunits and one γ subunit (reviewed by Olsen, 2018). Importantly, the specific subunit composition of a given receptor directly determines specific functional properties, including kinetics (onset, decay) and single-channel conductance (reviewed by Hevers & Lüddens, 1998; Smart, 2015). For the large majority of defined cell types in the CNS, both local interneurons and long-axon projection neurons, there is overall little information about the expression and molecular composition of specific GABA$_A$ receptors that mediate inhibitory input, irrespective of whether it is synaptic, extrasynaptic or both. Such information is important for understanding the contribution to the specific signal processing tasks of different types of neurons in the neural microcircuits in which they are found.

5.1 | GABAergic synapses on A17 amacrine cells

In this study, we found direct evidence for GABAergic spIPSCs. They were completely and reversibly blocked by a low concentration (3 μM) of the specific GABA$_A$ receptor antagonist SR95531, consistent with the spIPSCs being mediated by conventional (low-affinity) GABA$_A$ receptors typically found at GABAergic synapses. For A17 amacrine cells, ultrastructural investigations in cat retina found strong evidence for input from other types of amacrine cells located at the proximal dendrites, both at varicosities and at intervaricosity segments (Nelson & Kolb, 1985). It is as yet unknown to which amacrine cells the presynaptic profiles and processes belong, but it is

reasonable to assume that they are either GABAergic or glycinergic inputs from wide-field or narrow-field amacrine cells, respectively. The spatial distribution and segregation of inhibitory (from amacrine cells) and excitatory (from rod bipolar cells) inputs seem to be characteristic features of the A17 cells. The excitatory input is located at the dendritic varicosities at the middle and distal parts of the dendrites and seems to originate exclusively from the axon terminals of rod bipolar cells (Nelson & Kolb, 1985; Zhang et al., 2002).

The biophysical properties of the GABAergic spIPSCs seem overall consistent with a relatively proximal location of the corresponding synapses. Given the extremely small diameters of the A17 dendrites between the dendritic varicosities (Ellias & Stevens, 1980; Grimes et al., 2010), we would expect strong electrotonic attenuation from dendritic filtering of spIPSCs generated at distal dendritic locations. The fact that few spIPSCs with evidence for strong dendritic filtering (low amplitudes combined with very slow rise and decay times) were observed cannot be taken as evidence for the absence of inhibitory synapses in the distal dendrites, as the electrotonic filtering could be so strong as to essentially make the spIPSCs appear as current noise. In contrast, however, the observations of spIPSCs with very fast rise times suggest that at least some of the recorded spIPSCs originated at locations relatively close to the soma. In the absence of compartmental models developed from morphologically realistic reconstructions and physiological measurements, a more precise analysis cannot yet be performed. For such compartmental modelling, it is a limitation of our study that the physiological measurements were performed at room temperature (22–25°C). The temperature dependence of synaptic kinetics tends to be steep, typically with a Q_{10} temperature coefficient (the experimentally determined change for a 10°C difference in temperature) of 2–3 (Hille, 2001; Roth & van Rossum, 2010). In contrast, the Q_{10} of the conductance of an open ion channel is much lower, typically only 1.2–1.5 (Hille, 2001). Ideally, Q_{10} values for synaptic kinetics and amplitude should be determined experimentally, but it can be a problem to obtain adequate kinetic data because of electrotonic filtering that effectively sets a lower limit for experimentally determined values. Alternatively, the kinetic data can be scaled by default values for Q_{10}.

Several observations in our study provide information about the potential subunit composition of the synaptic GABA$_A$ receptors of A17 amacrines. First, whereas GABA$_A$ receptors that only contain αβ subunits have a single-channel conductance of 11–15 pS, those containing the αβδ or αβγ subunits have conductances of 24–28 pS (Angelotti & Macdonald, 1993; Brickley et al., 1999; Fisher & Macdonald, 1997; Mortensen & Smart, 2006).

With non-stationary noise analysis of spIPSCs from A17 amacrines, we obtained an average single-channel conductance of ~21 pA. Even though the range was larger (~17 to ~28 pS), it is likely that electrotonic filtering would reduce the apparent conductance values (cf. Hartveit & Veruki, 2006). Accordingly, we consider the most likely interpretation to be that the receptors contain αβγ subunits, as receptors with the αβδ composition are predominantly extrasynaptic. The αβγ subunit combination is the most common for synaptic receptors and display fast kinetics. It is difficult to predict the interaction between synaptic excitation and inhibition in A17 amacrines, in particular because we do not know the exact spatial location of the inhibitory input. If no inhibitory inputs target the distal regions of the dendritic tree, it is possible that the strongest influence of the inhibition will be to prevent spread of excitatory inputs in the distal dendrites to the soma region, and from there, the spread into other major dendritic branches and subtrees. If enhancing the extent of compartmentalization is an important function of synaptic inhibition in A17s, it suggests that, at least under certain circumstances (e.g. with higher levels of excitatory input from rod bipolar cells to A17s), there could be consequential spread of excitation along the dendrites of A17 amacrine cells (cf. Grimes et al., 2009, 2010). It will be important for future work to map the dendritic location of GABAergic (as well as potential glycinergic) synaptic inputs and to develop realistic compartmental models, based on quantitative morphological reconstruction, that can be used for studying signal integration in A17 amacrine cells.

The variability observed for the kinetics and amplitude properties of the GABAergic spIPSCs in A17 amacrines can probably to some extent be accounted for by variability in electrotonic filtering, that is, because the spIPSCs were generated at different distances from the cell body where the recording pipette was located. Alternatively, it is also possible that some of the variability observed for the spIPSCs could be caused by variability of the spatiotemporal neurotransmitter concentration profile (peak, decay, clearance) in the synaptic cleft, both within and between different synapses. Current estimates of the peak concentration of GABA in the synaptic cleft after release of a single vesicle range between ~500 μM and 3–5 mM (Maconochie et al., 1994; Overstreet et al., 2002; for review, see Clements, 1996; Mody et al., 1994; Scimemi & Beato, 2009).

For the A17 amacrine cells, the responses we obtained with ultra-fast application of brief pulses of GABA to outside-out patches displayed slower decay kinetics than observed for the spIPSCs. There are multiple explanations for this difference. First, it is possible that the receptor subunit composition of the synaptic receptors is different from that of the extrasynaptic

(somatic) receptors and that this impacts the decay kinetics observed under the experimental conditions employed here. Our pharmacological experiments suggested that the synaptic receptors correspond to an α1βγ2 combination, whereas the extrasynaptic somatic receptors correspond to an α2βγ2 and/or an α3βγ2 combination. Notably, α1-containing receptors are considered to display faster deactivation than both α2- and α3-containing receptors (reviewed by Smart, 2015). Second, even in a situation with identical subunit composition of synaptic and extrasynaptic receptors, it is possible that differences in decay kinetics could be explained by differences in post-translational modification, including the state of phosphorylation (for review, see Nakamura et al., 2015). Third, a potentially confounding problem for interpreting the difference in decay kinetics is that when we measured the deactivation kinetics in patch experiments, even the duration of the briefest GABA pulses (2–3 ms) was longer than the brief synaptic transients likely to exist in the synaptic cleft (Clements, 1996). This means that a larger fraction of receptors might be driven into one or more desensitized states, from which they can later enter the open state(s) and thereby prolong the deactivation time course (cf. Jones & Westbrook, 1996).

5.2 | Extrasynaptic GABA$_A$ receptors on A17 amacrine cells

Because there is no evidence for synaptic inputs directly onto the cell bodies of A17 amacrines, we consider the GABA$_A$ receptors in the somatic patches to be extrasynaptic. In addition to the difference in decay kinetics of the spIPSCs and the deactivation kinetics for the brief pulse responses of the outside-out patches, we observed a difference in the effects of Zn^{2+} and zolpidem between the two types of receptors. For Zn^{2+}, we observed that a low concentration of 10 μM strongly suppressed the GABA-evoked patch responses, but not the GABAergic spIPSCs. For the benzodiazepine agonist zolpidem, we observed that a low concentration of 100 nM increased the amplitude and markedly slowed the decay kinetics of the spIPSCs, but had no effect on the amplitude or decay kinetics of the patch responses. Taken together with other properties measured for the patch responses, this suggested that the extrasynaptic somatic receptors correspond to an α2βγ2 and/or an α3βγ2 combination.

It is an open question whether A17 amacrines also have extrasynaptic GABA$_A$ receptors along their dendrites and, if so, to which extent the properties of the somatic extrasynaptic receptors are representative of putative dendritic extrasynaptic receptors. Further work is required to provide answers to both questions. There are multiple examples where GABA$_A$ receptors have an extrasynaptic location and there is strong evidence that such receptors can play a functionally important role in many regions of the CNS by mediating tonic currents (for review, see Olsen, 2018). These tonic currents are generated by spillover of synaptically released GABA or by ambient concentrations of GABA in the extracellular environment. Importantly, the α subunit is a key determinant of the kinetic properties of GABA$_A$ receptors, and the α subunits of extrasynaptic GABA$_A$ receptors are primarily α4, α5 and α6. This contrasts with the α1, α2 and α3 subunits, which are most commonly found as part of synaptic receptors (Fritschy & Brünig, 2003; Möhler et al., 2004), although there are exceptions (e.g. Jia et al., 2005; Nusser et al., 1998; Sun et al., 2004). When specific types of GABA$_A$ receptors mediate tonic currents, they exhibit high affinity for GABA and slow desensitization. Across different regions and cell types, such tonic currents are generated by GABA$_A$ receptors that usually contain the α5 or δ subunit (reviewed by Bright & Smart, 2013; Farrant & Nusser, 2005). For A17 amacrine cells, we did not find evidence for the δ subunit in the extrasynaptic receptors of somatic patches, suggesting that these receptors do not mediate a tonic current driven by the ambient concentration of GABA. We cannot exclude, however, that potential extrasynaptic receptors elsewhere in the A17 amacrines might contain α5 or δ subunits, although there is evidence that the α5 subunit is not expressed in rat retina (Wässle et al., 1998) and that expression of the δ subunit is restricted to cholinergic amacrine cells (Brandstätter et al., 1995; Greferath et al., 1993, 1995).

5.3 | GABA receptors on A17 amacrine cells and the functional role of GABAergic synaptic input to A17 amacrine cells

The whole-cell recordings of A17s in slices in the current study provide direct evidence for synaptic input mediated by GABA$_A$ receptors. Based on the pharmacological properties of both the somatic and the synaptic receptors, they are 'classical' GABA$_A$ receptors, with no evidence for receptors with atypical pharmacology (non-A, non-B or GABA$_C$) made up of ρ subunits (potentially as homomeric receptors).

In light of the evidence for glycinergic spIPSCs in displaced A17 amacrines in mouse retina (Majumdar et al., 2009), it is puzzling that we did not find evidence for glycinergic spIPSCs in our recordings. This could, in principle, be related to a species difference, although we do not consider this possibility very likely. It is also

possible that under our recording conditions, potential presynaptic glycinergic neurons do not provide spontaneous input, but that such input might be observed if the general level of excitability is increased. Alternatively, it could be due to a difference between A17 amacrine cells with cell bodies located in the inner nuclear layer and displaced A17 amacrines with cell bodies in the ganglion cell layer. If we assume that at least the predominant GABAergic input to A17 amacrine cells is located at the proximal dendrites, the synapses will be located approximately in S1–S2 of the inner plexiform layer. If we also assume that the input is mediated by amacrine cells with morphology typical for GABAergic amacrine cells, that is, wide field, it is potentially difficult to envisage that the same type of wide-field GABAergic amacrine cell can provide morphologically and functionally equivalent presynaptic input to both the normal and displaced A17 amacrine cells. Further work is required to clarify these questions.

In addition to $GABA_A$ receptors, the possibility should also be considered that A17 amacrine cells might express metabotropic, that is, $GABA_B$ receptors. It is indeed intriguing that Koulen et al. (1998) found evidence for localization of $GABA_B$ receptors at amacrine cell processes that form reciprocal synapses with rod bipolar cells, but these have so far not been shown conclusively to be from A17 amacrine cells. To our knowledge, the presence of functional $GABA_B$ receptors on A17 amacrine cells remains to be investigated in physiological experiments, but an interesting possibility is that they could have a presynaptic localization and thereby function as autoreceptors, for example, to regulate release of GABA from the A17.

Although recent evidence has suggested a pronounced compartmentalization of signalling in the dendrites of A17 amacrine cells, potentially with a large number of independently operating microcircuits, with parallel processing linked to the functionally isolated dendritic varicosities (Chávez et al., 2006; Grimes et al., 2009, 2010), it has also been speculated that the signal processing in these cells could occur over larger dendritic regions (Bloomfield, 1992; Nelson & Kolb, 1985; Völgyi et al., 2002; Zhang et al., 2002), potentially with a modulatory control of the extent of spatial integration (local vs. global). Importantly, Grimes et al. (2009, 2010) suggested that such modulatory control could be mediated by the activation of BK-type channels. It is possible that GABAergic inhibition targeted to proximal dendritic regions could play an important role for enhancing the degree of functional compartmentalization and maintain the independence of the major dendrites, if not that of individual dendritic varicosities. An additional speculation is that the strength of inhibitory synaptic input targeting proximal dendritic segments could be important for controlling the extent of global integration in A17 amacrine cells. It will be important for future work to determine the location of GABAergic synaptic input to A17 amacrines, for example, by two-photon uncaging with mapping of synaptic 'hot spots', immunolabelling of synaptic receptors and scaffolding proteins and large-scale ultrastructural reconstruction of A17 dendrites.

CONFLICT OF INTEREST
No conflicts of interest, financial or otherwise, are declared by the authors.

AUTHOR CONTRIBUTIONS
PB, AC and BT performed experiments; PB, AC, BT, MLV and EH analysed data; EH contributed analytic tools; PB, MLV and EH interpreted results; PB and MLV prepared figures; EH and MLV conceived and designed the research, supervised the project and wrote the manuscript. All authors approved the final version of the manuscript.

PEER REVIEW
The peer review history for this article is available at https://publons.com/publon/10.1111/ejn.15634.

DATA AVAILABILITY STATEMENT
The data that support the findings of this study are available from the corresponding authors upon reasonable request.

ORCID
Pablo Beltrán-Matas https://orcid.org/0000-0003-3817-5095
Áurea Castilho https://orcid.org/0000-0001-7012-5915
Barbora Tencer https://orcid.org/0000-0003-0685-9679
Margaret L. Veruki https://orcid.org/0000-0002-0532-144X
Espen Hartveit https://orcid.org/0000-0003-1798-1901

REFERENCES
Angelotti, T. P., & Macdonald, R. L. (1993). Assembly of $GABA_A$ receptor subunits: $\alpha_1\beta_1$ and $\alpha_1\beta_1\gamma_{2S}$ produce unique ion channels with dissimilar single-channel properties. *The Journal of Neuroscience*, *13*, 1429–1440. https://doi.org/10.1523/JNEUROSCI.13-04-01429.1993

Barberis, A., Petrini, E. M., & Cherubini, E. (2004). Presynaptic source of quantal size variability at GABAergic synapses in rat hippocampal neurons in culture. *European Journal of Neuroscience*, *20*, 1803–1810. https://doi.org/10.1111/j.1460-9568.2004.03624.x

Beltrán-Matas, P., Hartveit, E., & Veruki M. L. (2021). Different glutamate sources and endogenous co-agonists activate extrasynaptic NMDA receptors on amacrine cells of the rod pathway microcircuit. *European Journal of Neuroscience*, *54*, 4456–4474. https://doi.org/10.1111/ejn.15325

Bloomfield, S. A. (1992). Relationship between receptive and dendritic field size of amacrine cells in the rabbit retina. *Journal of Neurophysiology*, *68*, 711–725. https://doi.org/10.1152/jn.1992.68.3.711

Brandstätter, J. H., Greferath, U., Euler, T., & Wässle, H. (1995). Co-stratification of GABA$_A$ receptors with the directionally selective circuitry of the rat retina. *Visual Neuroscience*, *12*, 345–358. https://doi.org/10.1017/S0952523800008026

Brickley, S. G., Cull-Candy, S. G., & Farrant, M. (1999). Single-channel properties of synaptic and extrasynaptic GABA$_A$ receptors suggest differential targeting of receptor subtypes. *The Journal of Neuroscience*, *19*, 2960–2973. https://doi.org/10.1523/JNEUROSCI.19-08-02960.1999

Bright, D. P., & Smart, T. G. (2013). Methods for recording and measuring tonic GABA$_A$ receptor-mediated inhibition. *Frontiers in Neural Circuits*, *7*, 193. https://doi.org/10.3389/fncir.2013.00193

Cardin, J. Á. (2018). Inhibitory interneurons regulate temporal precision and correlations in cortical circuits. *Trends in Neurosciences*, *41*, 689–700. https://doi.org/10.1016/j.tins.2018.07.015

Castilho, Á., Ambrósio, A. F., Hartveit, E., & Veruki, M. L. (2015). Disruption of a neural microcircuit in the rod pathway of the mammalian retina by diabetes mellitus. *Journal of Neuroscience*, *35*, 5422–5433. https://doi.org/10.1523/JNEUROSCI.5285-14.2015

Chávez, A. E., Singer, J. H., & Diamond, J. S. (2006). Fast neurotransmitter release triggered by Ca influx through AMPA-type glutamate receptors. *Nature*, *443*, 705–708. https://doi.org/10.1038/nature05123

Clements, J. D. (1996). Transmitter timecourse in the synaptic cleft: Its role in central synaptic function. *Trends in Neurosciences*, *19*, 163–171. https://doi.org/10.1016/S0166-2236(96)10024-2

Criswell, H. E., McCown, T. J., Moy, S. S., Mueller, R. A., Morrow, A. L., & Breese, G. R. (1997). Action of zolpidem on responses to GABA in relation to mRNAs for GABA$_A$ receptor alpha subunits within single cells: Evidence for multiple functional GABA$_A$ isoreceptors on individual neurons. *Neuropharmacology*, *12*, 1641–1652.

Dämgen, K., & Lüddens, H. (1999). Zaleplon displays a selectivity to recombinant GABA$_A$ receptors different from zolpidem, zopiclone and benzodiazepines. *Neuroscience Research Communications*, *25*, 139–148. https://doi.org/10.1002/(SICI)1520-6769(199911/12)25:3<139::AID-NRC3>3.0.CO;2-W

Diamond, J. S. (2017). Inhibitory interneurons in the retina: Types, circuitry, and function. *Annual Review of Vision Science*, *3*, 1–24. https://doi.org/10.1146/annurev-vision-102016-061345

Diamond, J. S., & Grimes, W. N. (2014). Distributed parallel processing in retinal amacrine cells. In H. Cuntz, M. W. Remme, & B. Torben-Nielsen (Eds.), *The computing dendrite: From structure to function* (pp. 191–204). Springer.

Draguhn, A., Verdorn, T. A., Ewert, M., Seeburg, P. H., & Sakmann, B. (1990). Functional and molecular distinction between recombinant rat GABA$_A$ receptor subtypes by Zn^{2+}. *Neuron*, *5*, 781–788. https://doi.org/10.1016/0896-6273(90)90337-F

Eggers, E. D., & Lukasiewicz, P. D. (2006). GABA$_A$, GABA$_C$ and glycine receptor-mediated inhibition differentially affects light-evoked signalling from mouse retinal rod bipolar cells. *The Journal of Physiology*, *572*, 215–225. https://doi.org/10.1113/jphysiol.2005.103648

Eggers, E. D., & Lukasiewicz, P. D. (2010). Interneuron circuits tune inhibition in retinal bipolar cells. *Journal of Neurophysiology*, *103*, 25–37. https://doi.org/10.1152/jn.00458.2009

Elgueta, C., Leroy, F., Vielma, A. H., Schmachtenberg, O., & Palacios, A. G. (2018). Electrical coupling between A17 cells enhances reciprocal inhibitory feedback to rod bipolar cells. *Scientific Reports*, *8*, 3123. https://doi.org/10.1038/s41598-018-21119-0

Ellias, S. A., & Stevens, J. K. (1980). The dendritic varicosity: A mechanism for electrically isolating the dendrites of cat retinal amacrine cells? *Brain Research*, *196*, 365–372. https://doi.org/10.1016/0006-8993(80)90401-1

Farrant, M., & Nusser, Z. (2005). Variations on an inhibitory theme: Phasic and tonic activation of GABA$_A$ receptors. *Nature Reviews Neuroscience*, *6*, 215–229. https://doi.org/10.1038/nrn1625

Feigenspan, A., Gustincich, S., & Raviola, E. (2000). Pharmacology of GABA$_A$ receptors of retinal dopaminergic neurons. *Journal of Neurophysiology*, *84*, 1697–1707. https://doi.org/10.1152/jn.2000.84.4.1697

Fisher, J. L., & Macdonald, R. L. (1997). Single channel properties of recombinant GABA$_A$ receptors containing γ_2 or δ subtypes expressed with α_1 and β_3 subtypes in mouse L929 cells. *The Journal of Physiology*, *505*, 283–297. https://doi.org/10.1111/j.1469-7793.1997.283bb.x

Franke, K., & Baden, T. (2017). General features of inhibition in the inner retina. *The Journal of Physiology*, *595*, 5507–5515. https://doi.org/10.1113/JP273648

Franke, K., Berens, P., Schubert, T., Bethge, M., Euler, T., & Baden, T. (2017). Inhibition decorrelates visual feature representations in the inner retina. *Nature*, *542*, 439–444. https://doi.org/10.1038/nature21394

Fritschy, J. M., & Brünig, I. (2003). Formation and plasticity of GABAergic synapses: Physiological mechanisms and pathophysiological implications. *Pharmacology & Therapeutics*, *98*, 299–323. https://doi.org/10.1016/S0163-7258(03)00037-8

Gao, H., & Smith, B. N. (2010). Zolpidem modulation of phasic and tonic GABA currents in the rat dorsal motor nucleus of the vagus. *Neuropharmacology*, *58*, 1220–1227. https://doi.org/10.1016/j.neuropharm.2010.03.003

Gardner, S. M., Trussell, L. O., & Oertel, D. (1999). Time course and permeation of synaptic AMPA receptors in cochlear nuclear neurons correlate with input. *The Journal of Neuroscience*, *19*, 8721–8729. https://doi.org/10.1523/JNEUROSCI.19-20-08721.1999

Gill, S. B., Veruki, M. L., & Hartveit, E. (2006). Functional properties of spontaneous IPSCs and glycine receptors in rod amacrine

(AII) cells in the rat retina. *The Journal of Physiology*, *575*, 739–759. https://doi.org/10.1113/jphysiol.2006.112839

Glowatzki, E., & Fuchs, P. A. (2002). Transmitter release at the hair cell ribbon synapse. *Nature Neuroscience*, *5*, 147–154. https://doi.org/10.1038/nn796

Greferath, U., Grünert, U., Fritschy, J. M., Stephenson, A., Möhler, H., & Wässle, H. (1995). GABA_A receptor subunits have differential distributions in the rat retina: In situ hybridization and immunohistochemistry. *The Journal of Comparative Neurology*, *353*, 553–571. https://doi.org/10.1002/cne.903530407

Greferath, U., Grünert, U., Möhler, H., & Wässle, H. (1993). Cholinergic amacrine cells of the rat retina express the δ-subunit of the GABA_A receptor. *Neuroscience Letters*, *163*, 71–73. https://doi.org/10.1016/0304-3940(93)90231-9

Grimes, W. N., Hoon, M., Briggman, K. L., Wong, R. O., & Rieke, F. (2014). Cross-synaptic synchrony and transmission of signal and noise across the mouse retina. *eLife*, *3*, e03892.

Grimes, W. N., Li, W., Chávez, A. E., & Diamond, J. S. (2009). BK channels modulate pre- and postsynaptic signaling at reciprocal synapses in retina. *Nature Neuroscience*, *12*, 585–592. https://doi.org/10.1038/nn.2302

Grimes, W. N., Zhang, J., Graydon, C. W., Kachar, B., & Diamond, J. S. (2010). Retinal parallel processors: More than 100 independent microcircuits operate within a single interneuron. *Neuron*, *65*, 873–885. https://doi.org/10.1016/j.neuron.2010.02.028

Grünert, U., & Hughes, T. E. (1993). Immunohistochemical localization of GABA_A receptors in the scotopic pathway of the cat retina. *Cell and Tissue Research*, *274*, 267–277. https://doi.org/10.1007/BF00318746

Gustincich, S., Feigenspan, A., Sieghart, W., & Raviola, E. (1999). Composition of the GABA_A receptors of retinal dopaminergic neurons. *The Journal of Neuroscience*, *19*, 7812–7822. https://doi.org/10.1523/JNEUROSCI.19-18-07812.1999

Gutiérrez, A., Khan, Z. U., & de Blas, A. L. (1996). Immunocytochemical localization of the α_6 subunit of the γ-aminobutyric acid_A receptor in the rat nervous system. *The Journal of Comparative Neurology*, *365*, 504–510. https://doi.org/10.1002/(SICI)1096-9861(19960212)365:3<504::AID-CNE12>3.0.CO;2-Q

Hartveit, E. (1999). Reciprocal synaptic interactions between rod bipolar cells and amacrine cells in the rat retina. *Journal of Neurophysiology*, *81*, 2923–2936. https://doi.org/10.1152/jn.1999.81.6.2923

Hartveit, E., & Veruki, M. L. (2006). Studying properties of neurotransmitter receptors by non-stationary noise analysis of spontaneous synaptic currents. *The Journal of Physiology*, *574*, 751–785. https://doi.org/10.1113/jphysiol.2006.111856

Hartveit, E., & Veruki, M. L. (2007). Studying properties of neurotransmitter receptors by non-stationary noise analysis of spontaneous postsynaptic currents and agonist-evoked responses in outside-out patches. *Nature Protocols*, *2*, 434–448. https://doi.org/10.1038/nprot.2007.47

Hartveit, E., Zandt, B.-J., Madsen, E., Castilho, Á., Mørkve, S. H., & Veruki, M. L. (2018). AMPA receptors at ribbon synapses in the mammalian retina: Kinetic models and molecular identity. *Brain Structure & Function*, *223*, 769–804. https://doi.org/10.1007/s00429-017-1520-1

Heinemann, S. H., & Conti, F. (1992). Nonstationary noise analysis and application to patch clamp recordings. *Methods in Enzymology*, *207*, 131–148. https://doi.org/10.1016/0076-6879(92)07009-D

Helmstaedter, M., Briggman, K. L., Turaga, S. C., Jain, V., Seung, H. S., & Denk, W. (2013). Connectomic reconstruction of the inner plexiform layer in the mouse retina. *Nature*, *500*, 168–174. https://doi.org/10.1038/nature12346

Hevers, W., & Lüddens, H. (1998). The diversity of GABA_A receptors. Pharmacological and electrophysiological properties of GABA_A channel subtypes. *Molecular Neurobiology*, *18*, 35–86. https://doi.org/10.1007/BF02741459

Hille, B. (2001). *Ion channels of excitable membranes* (3rd ed.). Sunderland.

Jia, F., Pignataro, L., Schofield, C. M., Yue, M., Harrison, N. L., & Goldstein, P. A. (2005). An extrasynaptic GABA_A receptor mediates tonic inhibition in thalamic VB neurons. *Journal of Neurophysiology*, *94*, 4491–4501. https://doi.org/10.1152/jn.00421.2005

Jonas, P. (1995). Fast application of agonists to isolated membrane patches. In B. Sakmann & E. Neher (Eds.), *Single-channel recording* (2nd ed.) (pp. 231–243). Plenum Press.

Jones, M. V., & Westbrook, G. L. (1995). Desensitized states prolong GABA_A channel responses to brief agonist pulses. *Neuron*, *15*, 181–191. https://doi.org/10.1016/0896-6273(95)90075-6

Jones, M. V., & Westbrook, G. L. (1996). The impact of receptor desensitization on fast synaptic transmission. *Trends in Neurosciences*, *19*, 96–101. https://doi.org/10.1016/S0166-2236(96)80037-3

Jones, M. V., & Westbrook, G. L. (1997). Shaping of IPSCs by endogenous calcineurin activity. *The Journal of Neuroscience*, *17*, 7626–7633. https://doi.org/10.1523/JNEUROSCI.17-20-07626.1997

Juhász, G., Kékesi, K. A., Nyitrai, G., Dobolyi, A., Krogsgaard-Larsen, P., & Schousboe, A. (1997). Differential effects of nipecotic acid and 4,5,6,7-tetrahydroisoxazolo[4,5-c]pyridin-3-ol on extracellular γ-aminobutyrate levels in rat thalamus. *European Journal of Pharmacology*, *331*, 139–144. https://doi.org/10.1016/S0014-2999(97)01044-3

Keller, C. A., Yuan, X., Panzanelli, P., Martin, M. L., Alldred, M., Sassoè-Pognetto, M., & Lüscher, B. (2004). The γ2 subunit of GABA_A receptors is a substrate for palmitoylation by GODZ. *The Journal of Neuroscience*, *24*, 5881–5891. https://doi.org/10.1523/JNEUROSCI.1037-04.2004

Khan, Z. U., Gutiérrez, A., Mehta, A. K., Miralles, C. P., & de Blas, A. L. (1996). The α4 subunit of the GABA_A receptors from rat brain and retina. *Neuropharmacology*, *35*, 1315–1322. https://doi.org/10.1016/S0028-3908(96)00033-0

Koulen, P., Malitschek, B., Kuhn, R., Bettler, B., Wässle, H., & Brandstätter, J. H. (1998). Presynaptic and postsynaptic localization of GABA_B receptors in neurons of the rat retina. *European Journal of Neuroscience*, *10*, 1446–1456. https://doi.org/10.1046/j.1460-9568.1998.00156.x

Legendre, P. (1999). Voltage dependence of the glycine receptor-channel kinetics in the zebrafish hindbrain. *Journal of Neurophysiology*, *82*, 2120–2129. https://doi.org/10.1152/jn.1999.82.5.2120

Lewis, C. A., & Faber, D. S. (1993). GABA responses and their partial occlusion by glycine in cultured rat medullary neurons.

Neuroscience, *52*, 83–96. https://doi.org/10.1016/0306-4522(93)90184-H

MacNeil, M. A., & Masland, R. H. (1998). Extreme diversity among amacrine cells: Implications for function. *Neuron*, *20*, 971–982.

Maconochie, D. J., Zempel, J. M., & Steinbach, J. H. (1994). How quickly can GABA$_A$ receptors open? *Neuron*, *12*, 61–71. https://doi.org/10.1016/0896-6273(94)90152-X

Majumdar, S., Weiss, J., & Wässle, H. (2009). Glycinergic input of widefield, displaced amacrine cells of the mouse retina. *The Journal of Physiology*, *587*, 3831–3849. https://doi.org/10.1113/jphysiol.2009.171207

Marc, R. E., & Liu, W.-L. S. (2000). Fundamental GABAergic amacrine cell circuitries in the retina: Nested feedback, concatenated inhibition, and axosomatic synapses. *The Journal of Comparative Neurology*, *425*, 560–582. https://doi.org/10.1002/1096-9861(20001002)425:4<560::AID-CNE7>3.0.CO;2-D

Marowsky, A., & Vogt, K. E. (2014). Delta-subunit-containing GABA$_A$-receptors mediate tonic inhibition in paracapsular cells of the mouse amygdala. *Frontiers in Neural Circuits*, *8*, 27. https://doi.org/10.3389/fncir.2014.00027

Meera, P., Wallner, M., & Otis, T. S. (2011). Molecular basis for the high THIP/gaboxadol sensitivity of extrasynaptic GABA$_A$ receptors. *Journal of Neurophysiology*, *106*, 2057–2064. https://doi.org/10.1152/jn.00450.2011

Menger, N., & Wässle, H. (2000). Morphological and physiological properties of the A17 amacrine cell in the rat retina. *Visual Neuroscience*, *17*, 769–780. https://doi.org/10.1017/S0952523800175108

Mody, I., de Koninck, Y., Otis, T. S., & Soltesz, I. (1994). Bridging the cleft at GABA synapses in the brain. *Trends in Neurosciences*, *17*, 517–525. https://doi.org/10.1016/0166-2236(94)90155-4

Möhler, H. (2006). GABA$_A$ receptor diversity and pharmacology. *Cell and Tissue Research*, *326*, 505–516. https://doi.org/10.1007/s00441-006-0284-3

Möhler, H., Fritschy, J. M., Crestani, F., Hensch, T., & Rudolph, U. (2004). Specific GABA$_A$ circuits in brain development and therapy. *Biochemical Pharmacology*, *68*, 1685–1690. https://doi.org/10.1016/j.bcp.2004.07.025

Mortensen, M., & Smart, T. G. (2006). Extrasynaptic αβ subunit GABA$_A$ receptors on rat hippocampal pyramidal neurons. *The Journal of Physiology*, *577*, 841–856. https://doi.org/10.1113/jphysiol.2006.117952

Nakamura, Y., Darnieder, L. M., Deeb, T. Z., & Moss, S. J. (2015). Regulation of GABA$_A$Rs by phosphorylation. *Advances in Pharmacology*, *72*, 97–146. https://doi.org/10.1016/bs.apha.2014.11.008

Nelson, R., & Kolb, H. (1985). A17: A broad-field amacrine cell in the rod system of the cat retina. *Journal of Neurophysiology*, *54*, 592–614. https://doi.org/10.1152/jn.1985.54.3.592

Nusser, Z., Cull-Candy, S., & Farrant, M. (1997). Differences in synaptic GABA$_A$ receptor number underlie variation in GABA mini amplitude. *Neuron*, *19*, 697–709. https://doi.org/10.1016/S0896-6273(00)80382-7

Nusser, Z., Sieghart, W., & Somogyi, P. (1998). Segregation of different GABA$_A$ receptors to synaptic and extrasynaptic membranes of cerebellar granule cells. *The Journal of Neuroscience*, *18*, 1693–1703. https://doi.org/10.1523/JNEUROSCI.18-05-01693.1998

Olsen, R. W. (2018). GABA$_A$ receptor: Positive and negative allosteric modulators. *Neuropharmacology*, *136*, 10–22. https://doi.org/10.1016/j.neuropharm.2018.01.036

Otis, T. S., Wu, Y. C., & Trussell, L. O. (1996). Delayed clearance of transmitter and the role of glutamate transporters at synapses with multiple release sites. *The Journal of Neuroscience*, *16*, 1634–1644. https://doi.org/10.1523/JNEUROSCI.16-05-01634.1996

Overstreet, L. S., Westbrook, G. L., & Jones, M. V. (2002). Measuring and modeling the spatiotemporal profile of GABA at the synapse. In M. W. Quick (Ed.), *Transmembrane transporters* (pp. 259–275). Wiley-Liss.

Palay, S. L., & Chan-Palay, V. (1974). *Cerebellar cortex: Cytology and organization*. Springer-Verlag.

Park, S. J. H., Lieberman, E. E., Ke, J.-B., Rho, N., Ghorbani, P., Rahmani, P., Jun, N. Y., Lee, H.-L., Kim, I.-J., Briggman, K. L., Demb, J. B., & Singer, J. H. (2020). Connectomic analysis reveals an interneuron with an integral rol in the retinal circuit for night vision. *eLife*, *9*, e56077. https://doi.org/10.7554/eLife.56077

Poleg-Polsky, A., Ding, H., & Diamond, J. S. (2018). Functional compartmentalization within starburst amacrine cell dendrites in the retina. *Cell Reports*, *22*, 2898–2908. https://doi.org/10.1016/j.celrep.2018.02.064

Pritchett, D. B., & Seeburg, P. H. (1990). γ-Aminobutyric acid$_A$ receptor α$_5$-subunit creates novel type II benzodiazepine receptor pharmacology. *Journal of Neurochemistry*, *54*, 1802–1804. https://doi.org/10.1111/j.1471-4159.1990.tb01237.x

Pritchett, D. B., Sontheimer, H., Shivers, B. D., Ymer, S., Kettenmann, H., Schofield, P. R., & Seeburg, P. (1989). Importance of a novel GABA$_A$ receptor subunit for benzodiazepine pharmacology. *Nature*, *338*, 582–585. https://doi.org/10.1038/338582a0

Protti, D. A., Gerschenfeld, H. M., & Llano, I. (1997). GABAergic and glycinergic IPSCs in ganglion cells of rat retinal slices. *The Journal of Neuroscience*, *17*, 6075–6085. https://doi.org/10.1523/JNEUROSCI.17-16-06075.1997

Puia, G., Vicini, S., Seeburg, P. H., & Costa, E. (1991). Influence of recombinant γ-aminobutyric acid-$_A$ receptor subunit composition on the action of allosteric modulators of γ-aminobutyric acid-gated Cl$^-$ currents. *Molecular Pharmacology*, *39*, 691–696.

Rogers, C. J., Twyman, R. E., & Macdonald, R. L. (1994). Benzodiazepine and β-carboline regulation of single GABA$_A$ receptor channels of mouse spinal neurones in culture. *The Journal of Physiology*, *475*, 69–82. https://doi.org/10.1113/jphysiol.1994.sp020050

Roth, A., & van Rossum, M. C. W. (2010). Modeling synapses. In E. de Schutter (Ed.), *Computational modeling methods for neuroscientists* (pp. 139–159). MIT Press.

Scimemi, A., & Beato, M. (2009). Determining the neurotransmitter concentration profile at active synapses. *Molecular Neurobiology*, *40*, 289–306. https://doi.org/10.1007/s12035-009-8087-7

Smart, T. G. (2015). GABA$_A$ receptors. In J. Zheng & M. C. Trudeau (Eds.), *Handbook of ion channels* (pp. 345–359). CRC Press.

Smart, T. G., Moss, S. J., Xie, X., & Huganir, R. L. (1991). GABA$_A$ receptors are differentially sensitive to zinc: Dependence on subunit composition. *British Journal of Pharmacology*, *103*, 1837–1839. https://doi.org/10.1111/j.1476-5381.1991.tb12337.x

Stell, B. M., & Mody, I. (2002). Receptors with different affinities mediate phasic and tonic GABA$_A$ conductances in hippocampal neurons. *The Journal of Neuroscience*, *22*, RC223 (1-5).

Stórustovu, S., & Ebert, B. (2003). Gaboxadol: In vitro interaction studies with benzodiazepines and ethanol suggest functional selectivity. *European Journal of Pharmacology*, *467*, 49–56. https://doi.org/10.1016/S0014-2999(03)01603-0

Stórustovu, S., & Ebert, B. (2006). Pharmacological characterization of agonists at δ-containing GABA$_A$ receptors: Functional selectivity for extrasynaptic receptors is dependent on the absence of γ$_2$. *Journal of Pharmacology and Experimental Therapeutics*, *316*, 1351–1359.

Strettoi, E., Dacheux, R. F., & Raviola, E. (1990). Synaptic connections of rod bipolar cells in the inner plexiform layer of the rabbit retina. *The Journal of Comparative Neurology*, *295*, 449–466. https://doi.org/10.1002/cne.902950309

Strettoi, E., Raviola, E., & Dacheux, R. F. (1992). Synaptic connections of the narrow-field, bistratified rod amacrine cell (AII) in the rabbit retina. *The Journal of Comparative Neurology*, *325*, 152–168. https://doi.org/10.1002/cne.903250203

Sun, C., Sieghart, W., & Kapur, J. (2004). Distribution of α1, α4, γ2, and δ subunits of GABA$_A$ receptors in hippocampal granule cells. *Brain Research*, *1092*, 207–216.

Veruki, M. L., Mørkve, S. H., & Hartveit, E. (2003). Functional properties of spontaneous EPSCs and non-NMDA receptors in rod amacrine (AII) cells in the rat retina. *The Journal of Physiology*, *549*, 759–774. https://doi.org/10.1113/jphysiol.2003.039982

Veruki, M. L., Zhou, Y., Castilho, Á., Morgans, C. W., & Hartveit, E. (2019). Extrasynaptic NMDA receptors on rod pathway amacrine cells: Molecular composition, activation, and signaling. *The Journal of Neuroscience*, *39*, 627–650. https://doi.org/10.1523/JNEUROSCI.2267-18.2018

Völgyi, B., Xin, D., & Bloomfield, S. A. (2002). Feedback inhibition in the inner plexiform layer underlies the surround-mediated responses of AII amacrine cells in the mammalian retina. *The Journal of Physiology*, *539*, 603–614. https://doi.org/10.1113/jphysiol.2001.013133

Wafford, K. A., Whiting, P. J., & Kemp, J. A. (1993). Differences in affinity and efficacy of benzodiazepine receptor ligands at recombinant γ-aminobutyric acid$_A$ receptor subtypes. *Molecular Pharmacology*, *43*, 240–244.

Wässle, H., Koulen, P., Brandstätter, J. H., Fletcher, E. L., & Becker, C.-M. (1998). Glycine and GABA receptors in the mammalian retina. *Vision Research*, *38*, 1411–1430. https://doi.org/10.1016/S0042-6989(97)00300-3

Yan, W., Laboulaye, M. A., Tran, N. M., Whitney, I. E., Benhar, I., & Sanes, J. R. (2020). Mouse retinal cell atlas: Molecular identification of over sixty amacrine cell types. *The Journal of Neuroscience*, *40*, 5195–5177.

Zandt, B.-J., Liu, J. H., Veruki, M. L., & Hartveit, E. (2017). AII amacrine cells: Quantitative reconstruction and morphometric analysis of electrophysiologically identified cells in live retinal slices imaged with multi-photon excitation microscopy. *Brain Structure & Function*, *222*, 151–182. https://doi.org/10.1007/s00429-016-1206-0

Zhang, J., Jung, C. S., & Slaughter, M. M. (1997). Serial inhibitory synapses in retina. *Visual Neuroscience*, *14*, 553–563. https://doi.org/10.1017/S0952523800012219

Zhang, J., Li, W., Trexler, E. B., & Massey, S. C. (2002). Confocal analysis of reciprocal feedback at rod bipolar terminals in the rabbit retina. *The Journal of Neuroscience*, *22*, 10871–10882. https://doi.org/10.1523/JNEUROSCI.22-24-10871.2002

Zhang, S., & Trussell, L. O. (1994). A characterization of excitatory postsynaptic potentials in the avian nucleus magnocellularis. *Journal of Neurophysiology*, *72*, 705–718. https://doi.org/10.1152/jn.1994.72.2.705

Zhou, Y., Tencerova, B., Hartveit, E., & Veruki, M. L. (2016). Functional NMDA receptors are expressed by both AII and A17 amacrine cells in the rod pathway of the mammalian retina. *Journal of Neurophysiology*, *115*, 389–403. https://doi.org/10.1152/jn.00947.2015